UNIVERSIDADE
BEIRA INTERIOR

Lignin-based 3D scaffolds for bone tissue regeneration applications

Adriana Sofia da Silva Barroso

Dissertação para obtenção do Grau de Mestre em
Bioquímica
(2º ciclo de estudos)

Orientador: Professor Doutor Ilídio Joaquim Sobreira Correia
Co-orientador: Doutor André Ferreira Moreira
Co-orientador: Mestre Cátia Solange Duarte Cabral

Outubro de 2022

Declaração de Integridade

Eu, Adriana Sofia da Silva Barroso, que abaixo assino, estudante com o número de inscrição M11118 de Bioquímica da Faculdade Ciências, declaro ter desenvolvido o presente trabalho e elaborado o presente texto em total consonância com o **Código de Integridades da Universidade da Beira Interior**.

Mais concretamente afirmo não ter incorrido em qualquer das variedades de Fraude Académica, e que aqui declaro conhecer, que em particular atendi à exigida referenciação de frases, extratos, imagens e outras formas de trabalho intelectual, e assumindo assim na íntegra as responsabilidades da autoria.

Universidade da Beira Interior, Covilhã 06 / 10/ 2022

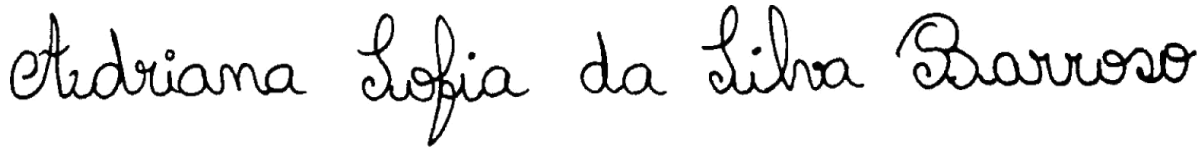

"Não vou dizer que é fácil e que nunca deu vontade de desistir, mas vale muito mais a pena continuar"

Caio Fernando Abreu

Dedication

Dedico este trabalho à minha família, em particular aos meus pais, à minha irmã, ao meu cunhado, aos meus lindos afilhados, Diogo e Inês, e aos meus avós, por todo o apoio, força e encorajamento que me deram ao longo da minha jornada académica.

Acknowledgments

Inicialmente, quero agradecer ao meu orientador, Professor Doutor Ilídio Correia, por me ter aceitado neste grupo de investigação e por me ter facultado os recursos necessários para o desenvolvimento da minha dissertação. Agradeço a sua orientação, conselhos e a sua exigência que promoveram a realização deste trabalho com sucesso.

Ao meu co-orientador, Doutor André Moreira, agradeço toda a ajuda, paciência e todo o tempo que disponibilizou-comigo ao longo desta tese. Desta forma, agradeço por todo o conhecimento que me transmitiu, pela motivação e por nunca me deixar desistir.

À minha co-orientadora Mestre Cátia Cabral, estou grata por toda a sua ajuda e conhecimentos que me transmitiu. Também quero agradecer pela paciência, e disponibilidade para me ajudar ao longo desta tese. Obrigada por tudo.

Um obrigado a todos os colegas de laboratório por me terem sempre ajudado quando precisei e pelo apoio que me proporcionaram.

Aos meus colegas de mestrado, Micaela, Francisco e André quero agradecer por todo o apoio, motivação e conselhos que me deram ao longo deste ano. Um especial agradecimento à Micaela por todas as conversas, por todas as companhias e pelas ajudas nas neutralizações. Tornaste uma grande amiga e ficarás sempre no meu coração.

À Rainha da casa, quero agradecer todas as horas que ficaste comigo até as tantas, por me ouvires e me aconselhares sempre que as coisas não estavam a correr da melhor maneira, e por todos nossos momentos divertidos que passamos juntas. Obrigada pela linda amizade que criámos ao longo destes 4 anos. Além disso, agradeço à Covilhã pelas pessoas incríveis que me deu: Maria, Belinha, Inês, Tatiana, afilhada Diana e afilhado Carlos. Obrigada por todo o apoio e motivação para que conseguisse sempre alcançar os meus sonhos. Sabem o quanto são importantes para mim e o quanto vos adoro.

Finalmente, quero agradecer à minha família por todo o apoio e força que me deram ao longo deste percurso académico. Por acreditarem sempre em mim e nunca me deixarem desistir dos meus sonhos, espero deixar-vos muito orgulhosos. Obrigada pelas nossas conversas longas para eu desabafar e para não me sentir sozinha. Sabem o quanto importante são para mim e quanto vos adoro, mesmo estando longe estão sempre comigo.

Por fim, um grande agradecimento a Deus.

Resumo

O osso é um tecido conjuntivo, vascularizado e mineralizado, que participa na proteção dos órgãos, no suporte e locomoção do corpo humano, na manutenção da homeostase e na hematopoiese. No entanto, ao longo da vida podem surgir defeitos ósseos causados por trauma (fraturas mecânicas), doença e/ou envelhecimento, que quando demasiado extensos comprometem a capacidade do osso se autorregenerar. Nestas circunstâncias, as lesões podem ser tratadas através dos diferentes tipos de enxertos, tais como os auto-, alo-, ou xenoenxertos. Contudo, estas abordagens apresentam algumas desvantagens como a disponibilidade limitada, a formação de novas lesões, e possibilidade de rejeição por parte do paciente. Desta forma, têm sido desenvolvidas novas abordagens terapêuticas, permanentes ou temporárias, para suportar e acelerar o processo de regeneração óssea. Particularmente, as técnicas de prototipagem rápida, que permitem a utilização de materiais compósitos (constituídos por cerâmica e polímeros), têm permitido o rápido desenvolvimento de estruturas 3D personalizadas e com propriedades osteoinductivas e osteocondutivas.

Com o intuito de reforçar as propriedades mecânicas e osteogénicas destas estruturas 3D, neste trabalho, desenvolveu-se um novo andaime 3D que foi produzido através da deposição camada a camada de uma mistura composta por fosfato de tricálcico (TCP), alginato de sódio (SA) e lignina (LG) utilizando a impressora *Fab@Home 3D-Plotter*. A composição da mistura impressa em 3D, *i.e.*, fase inorgânica e orgânica, teve por objetivo reproduzir a composição natural da matriz óssea. Para estudar o efeito da LG, foram produzidos três andaimes de TCP/LG/SA, variando o rácio entre LG e SA (1:3, 1:2 e 1:1) e comparados com os andaimes de TCP/SA. Os resultados obtidos demonstraram que as inclusões da LG contribuíram para uma melhoria na resistência mecânica dos andaimes, particularmente no rácio 1:2, e permitiu a otimização da hidrofilicidade dos materiais. Além disso, os andaimes TCP/LG/SA apresentaram uma elevada biocompatibilidade, durante os 7 dias de estudo, e permitiram a adesão e proliferação de osteoblastos humanos (hOB) na sua superfície. Por outro lado, não foram registadas diferenças significativas na deposição de cálcio à superfície dos andaimes de TCP/LG/SA, quando comparados com os formulados com TCP/SA. Em conclusão, os resultados obtidos revelaram que os andaimes produzidos possuem propriedades adequadas para aplicação na regeneração óssea, originando estruturas mais fortes mecanicamente e com ambientes mais adequados para a adesão e proliferação celular.

Palavras-chave

Andaimes;Lignina;Materiais Compósitos;Prototipagem Rápida;Regeneração Óssea

Resumo Alargado

O osso é um tecido conjuntivo, vascularizado e mineralizado, que se encontra sob constante remodelação ao longo da vida humana. O osso desempenha diversas funções no corpo humano, tais como: a proteção dos órgãos, a locomoção, a manutenção da homeostase do corpo (reserva de minerais), e também está envolvido na hematopoiese. No tecido ósseo podem-se identificar duas fases principais: a matriz inorgânica constituída principalmente por cristais de fosfato de cálcio sob a forma de hidroxiapatita, e uma matriz orgânica maioritariamente formada por fibras de colagénio tipo I. Apesar da capacidade de autorregeneração, quando os danos são demasiado extensos, a estrutura do osso pode ficar comprometida. De forma a tratar estas lesões, em meio clínico são usados diferentes tipos de enxertos, como os auto-, alo-, ou xenoenxertos. Contudo, estas abordagens apresentam algumas desvantagens como a disponibilidade limitada, a formação de novas lesões, e possibilidade de rejeição. Desta forma, têm sido desenvolvidas novas abordagens, baseadas na utilização de biomateriais e engenharia de tecidos, para aplicação em lesões ósseas. Particularmente, técnicas de prototipagem rápida apresentam a capacidade de corresponder às exigências associadas ao rápido desenvolvimento de estruturas 3D personalizadas e com propriedades osteoinductivas e osteocondutivas. Além disso, as metodologias existentes permitem a combinação de diferentes materiais, inorgânicos e orgânicos, bem como a incorporação imediata de células de forma a acelerar o processo de regeneração óssea.

No presente estudo, um novo andaime 3D foi produzido através da deposição camada a camada de uma mistura composta por fosfato de tricálcico (TCP), alginato de sódio (SA) e lignina (LG) utilizando a impressora Fab@Home 3D-Plotter. A composição da mistura impressa em 3D teve por objetivo reproduzir a composição natural da matriz óssea, na qual a componente inorgânica, o TCP, confere as propriedades mecânicas e osteogénicas, enquanto o SA foi selecionado devido à sua biocompatibilidade e biodegradabilidade, e a LG contribui para a melhoria das propriedades mecânicas. Para estudar o efeito da LG, foram produzidos três andaimes de TCP/LG/SA, variando o rácio entre LG e SA (1:3, 1:2 e 1:1) e comparados com os andaimes de TCP/SA. Os resultados obtidos demonstraram que a inclusão da LG provoca uma melhoria na resistência mecânica dos andaimes, particularmente no rácio 1:2 onde se verificou um aumento de 15 % na força compressiva. Além disso, também foi observada a otimização da hidrofilicidade dos materiais para valores próximos dos considerados ideais para a promoção da adesão celular. Por outro

lado, os andaimes TCP/LG/SA apresentaram uma elevada biocompatibilidade, durante os 7 dias, e permitiram a adesão e proliferação de células hOB na sua superfície. Contudo, não foram registadas diferenças significativas na deposição de cálcio à superfície dos andaimes de TCP/LG/SA, quando comparados com os formulados com TCP/SA. Em conclusão, os resultados obtidos nesta dissertação de mestrado apoiam a aplicação dos andaimes formulados com a mistura TCP/LG/SA na regeneração óssea, originando estruturas mais fortes mecanicamente e com ambientes mais adequados para a adesão e proliferação celular.

No futuro, serão realizados ensaios de avaliação da expressão osteopontina, osteocalcina e BMP-2 para confirmar as propriedades osteoinductivas e osteocondutivas dos andaimes *de* TCP/LG/SA. Além disso, o desempenho *in vivo* dos andaimes de TCP/LG/SA será avaliado de forma a validar o seu potencial para aplicações na regeneração óssea. A introdução de células e/ou moléculas bioativas (*p. ex.*, fatores de crescimento) à mistura de TCP/LG/SA antes do processo de impressão poderá também ser considerada de forma a melhorar a funcionalidade dos andaimes.

Abstract

The bone is a connective, vascularized, and mineralized tissue that participates in the protection of organs, support and locomotion of the human body, maintenance of homeostasis, and in hematopoiesis. However, throughout the lifetime, bone defects may arise caused by trauma (mechanical fractures), disease, and/or aging, which when too extensive compromise the ability of the bone to self-regenerate. In these circumstances, lesions can be treated through different types of grafts, such as auto-, allo-, or xenografts. However, these approaches have some disadvantages, such as limited availability, the formation of new lesions, and the possibility of rejection. Thus, new methodologies have been developed, permanent or temporary, to support and accelerate the process of bone regeneration. Particularly, rapid prototyping techniques using composite materials (consisting of ceramics and polymers) have been showing the ability to allow the rapid development of customized 3D structures with osteoinductive and osteoconductive properties.

In order to reinforce the mechanical and osteogenic properties of these 3D structures, herein, a new 3D scaffold was produced through the layer-by-layer deposition of a tricalcium phosphate (TCP), sodium alginate (SA), and lignin (LG) mixture using the Fab@Home 3D-Plotter. The composition of the 3D printed mixture, *i.e.*, inorganic and organic phases, mimicked the natural composition of the bone matrix. Three different TCP/LG/SA scaffolds were produced by varying the LG/SA ratio (*i.e.*, 1:3, 1:2, and 1:1) and compared with the TCP/SA scaffolds. The results demonstrated that the LG inclusion improved the mechanical resistance of the scaffolds, particularly in the 1:2 formulation, and improved the water contact angle (WCA). Furthermore, the TCP/LG/SA scaffolds presented high biocompatibility during the 7 days of study and supported the adhesion and proliferation of hOB cells. Additionally, no significant differences were observed in the calcium deposition on TCP/LG/SA scaffolds, when compared to the TCP/SA counterparts. In conclusion, the results support the application of TCP/LG/SA scaffolds in bone regeneration, originating stronger structures with more suitable environments for cell adhesion and proliferation.

Keywords

3D scaffolds, Bone regeneration, Composite Materials, Lignin, Rapid prototyping.

Index

Chapter 1

1. Introduction 2

1.1 Bone Tissue 2

1.2 Bone Anatomy and Morphology 2

1.3 Bone Histology 4

1.3.1 Bone Matrix 4

1.3.2 Bone cells 5

1.3.2.1 Osteoblasts 5

1.3.2.2 Bone lining cells 6

1.3.2.3 Osteocytes 6

1.2.3.4 Osteoclasts 6

1.4 Bone regeneration process 7

1.4.1 Primary (direct) bone healing 7

1.4.2 Secondary (indirect) bone healing 8

1.5 Bone Grafts 9

1.6 Tissue Engineering 10

1.6.1 Properties exhibited by 3D scaffolds aimed for bone regeneration 11

1.6.1.1 Biocompatibility 11

1.6.1.2 Biodegradability 11

1.6.1.3 Surface properties, osteoconductivity, and osteoinductivity 12

1.6.1.5 Porosity 12

1.6.1.6 Antibacterial activity 13

1.6.2 Techniques used for scaffold fabrication 13

1.6.2.1 Scaffold fabrication with a Fab@Home 3D Plotter 14

1.6.3 Biomaterials used for scaffold fabrication 15

1.6.3.1 Ceramics 15

1.6.3.1.1 Tricalcium phosphate 15
1.6.3.1.2 Hydroxyapatite 16
1.6.3.2 Polymers 16
1.6.3.2.1 Natural polymers 17
1.6.3.2.1.1 Sodium Alginate 17
1.6.3.2.1.2 Lignin 18
1.6.3.2.1.3 Collagen 18
1.6.3.2.1.4 Chitosan 19
1.6.3.2.2 Synthetic polymers 19
1.7 Aims 21

Chapter 2

2. Materials and Methods 24
2.1 Materials 24
2.2 Methods 24
2.2.1 Production of scaffolds 24
2.2.2 Characterization of the morphology of the 3D scaffolds 25
2.2.3 Characterization of the scaffolds' physicochemical 25
2.2.3.1 Attenuated Total Reflectance- Fourier Transform Infrared spectroscopy 25
2.2.3.2 Energy dispersive spectroscopic analysis 26
2.2.4 Characterization of the scaffolds' mechanical properties 26
2.2.5 Characterization of the scaffolds' swelling profile 27
2.2.6 Contact angle measurements 27
2.2.7 Evaluation of scaffolds' porosity 27
2.2.8 Analysis of the biodegradation profile of the scaffolds 28
2.2.9 Characterization of the scaffolds' biological properties 28
2.2.9.1 Evaluation of the scaffolds' effect on the viability and proliferation of hOB cells 28
2.2.9.2 Characterization of cell adhesion at the surface of the scaffolds 29

2.2.9.3 Evaluation *in vitro* biomineralization 29
2.2.10 Statistical analysis 29
Chapter 3
3. Results and Discussion 32
3.1 Morphological characterization of the scaffolds 32
3.2 Characterization of the scaffolds' physicochemical properties 34
3.2.1 ATR-FTIR analysis 34
3.2.2 Energy dispersive spectroscopy analysis 35
3.3 Characterization of the 3D scaffolds' mechanical properties 35
3.4 Evaluation of the 3D scaffolds' swelling profile 36
3.5 Determination of the 3D scaffolds' wettability 37
3.6 Evaluation of scaffolds' porosity 38
3.7 Characterization of biodegradation profile of the scaffolds 39
3.8 Characterization of the biological properties of the produced scaffolds 40
3.8.1 Evaluation of scaffolds' cytotoxic profile 40
3.8.2 Evaluation in vitro biomineralization 44
Chapter 4
4. Conclusion and Future Perspectives 48
Chapter 5
5. References 50
Appendix I 61

List of Figures

Figure 1. Illustration of the trabecular and cortical bone..... 2

Figure 2. Representation of the types of cells found in bone 5

Figure 3. Illustration of the typical indirect healing phases..... 8

Figure 4. Chemical formula of tricalcium phosphate.....16

Figure 5. Chemical structure of hydroxyapatite 16

Figure 6. Chemical structure of sodium alginate 17

Figure 7. Chemical structure of lignin 18

Figure 8. Chemical structure of collagen.....19

Figure 9. Chemical structure of chitosan 19

Figure 10. Chemical structure of poly(caprolactone)..... 20

Figure 11. Production and characterization of 3D scaffolds..... 33

Figure 12. ATR-FTIR analysis of TCP, SA, LG (A) and TCP/LG/SA_1:3, TCP/LG/SA_1:2, TCP/LG/SA_1:1, and TCP/SA scaffolds (B) 34

Figure 13. Characterization of the 3D scaffolds' Cs (A) and YM (B) 36

Figure 14. Characterization of the 3D scaffolds' physicochemical properties. 39

Figure 15. Evaluation of the 3D scaffolds' weight loss over time in the absence (A) or presence (B) of lysozyme..... 40

Figure 16. Optical microscopy images acquired to characterize cells' behaviour in contact with the produced scaffolds during 1, 3 and 7 days. 42

Figure 17. Characterization of the scaffolds' cytocompatibility 43

Figure 18. Characterization of the scaffolds' biomineralization 45

List of Tables

Table 1. Summary of the produced scaffolds and their composition. 25

Table 2. EDS analysis of the 3D printed scaffolds..... 35

List of Abbreviations

ALP	Alkaline Phosphatase
ARS	Alizarin Red S
ATR-FTIR	Attenuated Total Reflectance-Fourier Transformed Infrared Spectroscopy
BLCs	Bone Lining Cells
BMP	Bone Morphogenic Proteins
BTE	Bone Tissue Engineering
CAD	Computer Assisted Design
Cs	Compressive Strength
DMEM-F12	Dulbecco's Modified Eagle's Medium: Nutrient Mixture F-12
ECM	Extracellular Matrix
EDS	Energy Dispersive Spectroscopy
EDTA	Ethylenediamine Tetraacetic Acid
ER	Endoplasmic Reticulum
EtOH	Ethanol
HAp	Hydroxyapatite
hOB	Human Osteoblasts
IGFs	Insulin-Like Growth Factors
IL-1	Interleukin-1
IL-6	Interleukin-6
IL-11	Interleukin-11
IL-18	Interleukin-18
LG	Lignin
MSC	Mesenchymal Stem Cell
PCL	Poly(caprolactone)
PGA	Polyglycolic Acid
PLA	Polylactic Acid
PLGA	Poly(lactic-co-glycolic) Acid
RP	Rapid Prototyping
RT	Room Temperature
SA	Sodium Alginate
SBF	Simulated Body Fluid

SEM	Scanning Electron Microscopy
TBS	Tris-Buffered Saline
TCP	Tricalcium Phosphate
TCP/LG/SA	Tricalcium Phosphate/Lignin/Sodium Alginate
TCP/SA	Tricalcium Phosphate/Sodium Alginate
TE	Tissue Engineering
TGF-β	Transforming Growth Factor-β
WCA	Water Contact Angle
YM	Young's Modulus

Chapter 1

Introduction

1. Introduction

1.1 Bone Tissue

Bone is a mineralized, highly vascularized, and dynamic connective tissue that is under constant remodeling throughout human' life [1, 2]. The bone tissue is composed by inorganic and organic phases, which are comprised of the bone matrix (*e.g.,* protein fibers and hydroxyapatite crystals), water, and bone cells (*i.e.,* osteoblasts, osteoclasts, osteocytes, and bone lining cells) [3]. The rigidity and strength of this tissue allow the bone to provide structural support as well as protect vital organs (*e.g.*, brain, lungs, heart) and other tissues [4]. Moreover, the bones are also involved in locomotion, mineral homeostasis, and hematopoiesis [4, 5].

In the following sections, the bone's anatomy, constitution, and regeneration process are described in more detail. Furthermore, the application of tissue engineering solutions in the treatment of bone lesions is also highlighted.

1.2 Bone Anatomy and Morphology

The human skeleton in the adult state consists of up to 213 bones that can be classified based on their morphology, shape, and bone matrix [6].

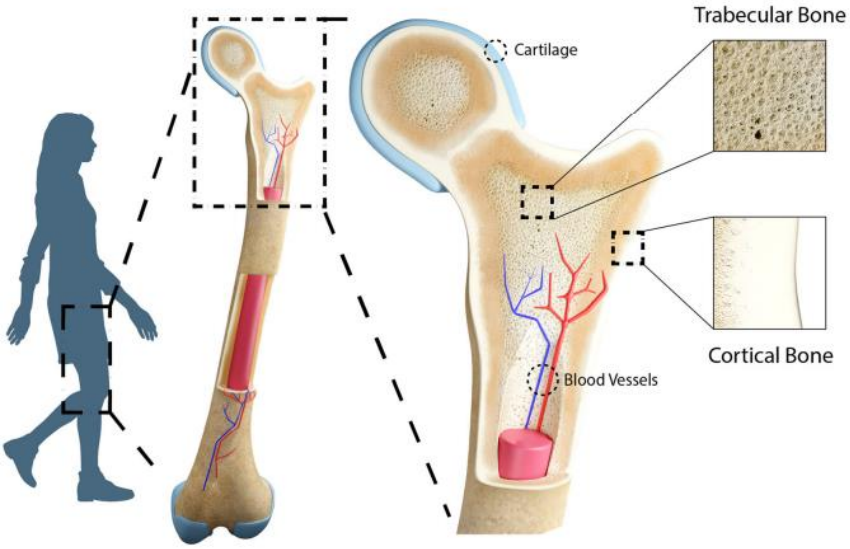

Figure 1. Illustration of the trabecular and cortical bone (adapted from [7]).

In terms of morphology, bone tissue is divided into cortical (compact) and trabecular (cancellous) bone, according to the ratio between the amount of bone matrix and void spaces within the bone (Figure 1). The adult human skeleton is composed of approximately 80 % cortical bone and 20 % trabecular bone, but this ratio can vary depending on the bone type and skeletal site [8, 9].

Cortical bone can be found on all bones, predominantly in the diaphysis of long bones, and represents most of human skeleton mass [8]. The cortical bone presents a dense, rigid, highly organized structure with a low porosity (≈ 10 %). Structurally, this type of bone is organized in cortical osteons, denominated as Haversian systems, that have a central canal or Havers (containing blood vessels responsible for the oxygen and nutrient exchange), surrounded by the concentric lamellae (osteons) [9-11]. The thickness and form of lamella in osteons may change from bone to bone and the location of the bone as well as the mechanical load. Particularly, the load-bearing bones present thicker and higher amounts of lamella. Moreover, the surface of cortical bone is also covered by the periosteum, a fibrous connective tissue that facilitates the fixation of tendons and ligaments to the bone [12].

Trabecular bone is made up of interconnected rods and plates called trabeculae, and between the trabeculae, some spaces are filled with bone marrow and blood vessels. Cancellous bone has a porous appearance (75 – 90 %), and due to its larger surface area, it has greater metabolic activity than cortical bone [13]. Furthermore, compared to cortical bone, trabecular bone is more active in remodeling, less mineralized (contains less calcium), and presents lower tissue density. In addition, collagen fibers are irregularly arranged, leading to lower mechanical strength. Trabecular bone is found in the extremities of long bones (femurs and humerus), in flat bones (jaw and skull), and in short bones (carpal and tarsal bones) [12, 14, 15].

Regarding, the shape of the bone, it can be classified as long, short, flat, or irregular [6]. Long bones are important because they support the body's weight and facilitate movement, being located in the lower or upper limbs. The long bones can be divided into three main components: 1) the diaphysis, which is primarily composed of compact bone; 2) epiphyses, which are primarily composed of cancellous bone; and 3) the epiphyseal plate, which is composed of hyaline cartilage, located between the epiphysis and the diaphysis, and is where length growth occurs [9].

Flat bones have neither diaphysis nor epiphysis and consist of two layers of compact bone that inside have a cancellous bone structure. This type of bone has the function of protecting internal organs, such as the brain (skull - occipital, parietal, frontal, nasal, lacrimal, and

vomer bones), the heart (rib cage - sternum and ribs), and the pelvic organs (pelvis - ilium, ischium, and pubis) [9].

Short and irregular bones are not elongated, so they do not have diaphysis. But certain regions of these bones have epiphyseal growth plates, containing small epiphyses. Examples of irregular bones are vertebrae, sacrum, coccyx, and hyoid bone, and for short bones, exists the carpal and tarsal bones, patellas, and sesamoid bones [9].

1.3 Bone Histology

1.3.1 Bone Matrix

The bone's extracellular matrix (ECM) consists of an inorganic phase (≈ 65 %), an organic phase (≈ 25 %), and water (≈ 10 %). These values may fluctuate with the person's age, nutrition, disease, and anti-osteoporotic treatments [16].

Collagen proteins represent approximately 90 % of the organic matrix, predominantly composed of type I collagen and, in lesser amounts, by type II and V collagen. These fibrillary proteins provide mechanical support, *i.e.,* flexible strength to the bone. Moreover, in the organic component can also be found other proteins such as osteocalcin, osteonectin, osteopontin, fibronectin, and bone sialoprotein II, that mainly play a structural, mechanical role and cell adhesion and migration. In turn, the proteoglycans, glycoproteins, growth factors (connective tissue growth factor and transforming growth factor-beta (TGF-β)), bone morphogenetic proteins (BMP-2 and BMP-7), and insulin-like growth factors (IGFs), are highly involved in biological processes, namely in cell attachment and differentiation, as well as in the deposition of minerals [17, 18].

The inorganic component of bone matrix consists mainly of calcium and phosphate minerals organized as hydroxyapatite. However, other inorganic elements (bicarbonate, sodium, citrate, magnesium, carbonate, fluorite, zinc, barium, and strontium) can be also present in this phase of the bone matrix [18, 19]. The calcium phosphate crystals nucleate with the collagen fibrils, which are parallelly arranged along the matrix, providing to the bone an increased stiffness and weight-bearing strength [20, 21].

The balance between the organic and inorganic phases is important to ensure appropriate bone flexibility and mechanical resistance. Reductions in the bone's inorganic content result

in a more flexible tissue due to the higher collagen ratio. In contrast, the bone becomes more fragile and brittle with the decrease in the collagen content [9].

1.3.2 Bone cells

The bone tissue is comprised of four different types of cells: i) osteoblasts; ii) bone lining cells; iii) osteocytes; and iv) osteoclasts, which through their coordinated action are fundamental for the bone maintenance and remodeling processes, represented in Figure 2.

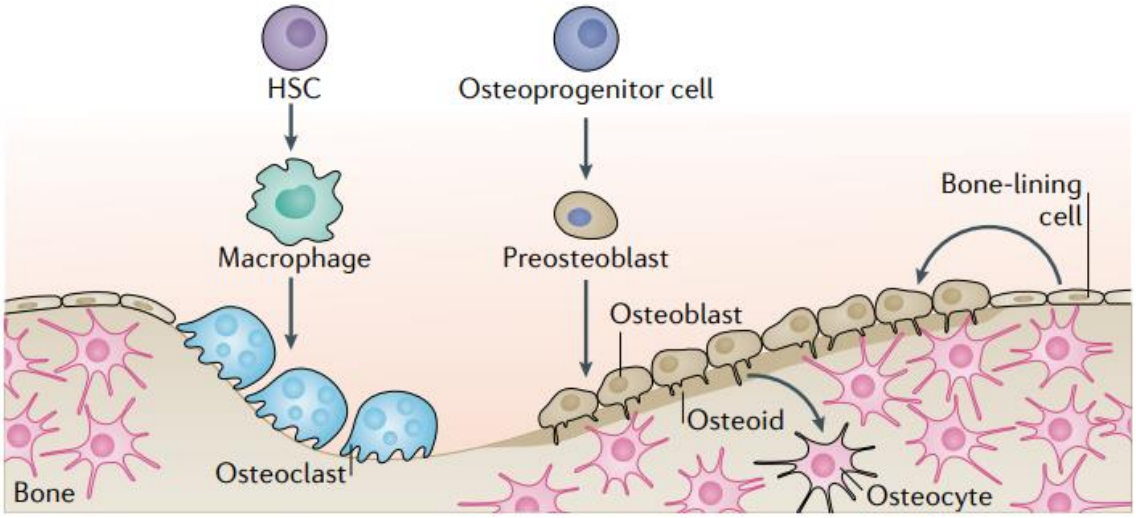

Figure 2. Representation of the types of cells found in bone (reproduced from [22]).

1.3.2.1 Osteoblasts

Osteoblasts are mononuclear cuboidal cells that are involved in the synthesis and organization of the bone's ECM. They derive from the mesenchymal stem cells (MSC) and are mainly located in the periosteum and bone marrow [23]. The osteoblasts are characterized by presenting large endoplasmic reticulum (ER) and a high number of ribosomes. The osteoblasts release two types of vesicles fundamental for the ossification process, one packed with collagen and proteoglycans, and the other, denominated as matrix vesicles, with high amounts of calcium (Ca^{2+}) and phosphate (PO_4^{3-}). When the ions concentration reaches a threshold is triggered the formation of hydroxyapatite crystals and the consequent bone ossification [24, 25] .

The matured osteoblasts can have three different fates, *i.e.*, i) they can be incorporated into the bone matrix and differentiate into osteocytes, ii) become quiescent lining cells, or iii) undergo programmed cell death [26].

1.3.2.2 Bone lining cells

Bone lining cells (BLCs) are quiescent osteoblasts located on the surface of the bone, that present a long, slender, and flat morphology. Another difference, when compared to osteoblast, is the phenotype of BLCs that express intercellular-1 adhesion molecules instead of osteocalcin [27, 28]. Although the role of BLCs is still not known with certainty, recent studies have shown that possibly these cells may be involved in the regulation of calcium homeostasis, bone remodeling process, and hematopoiesis, through the communication with osteoclasts via gap junctions [28]. Moreover, BLCs are also associated with the removal of non-mineralized collagen fibrils (expression of matrix metalloproteinases) and deposition of a smooth layer of collagen at the end of the remodeling phase [28, 29].

1.3.2.3 Osteocytes

Osteocytes are the most abundant cells in the bone tissue, differentiated from osteoblasts, and present in the bone lacunae surrounded by mineralized bone matrix [30, 31]. The osteocytes have a star-shaped morphology with several long and thin dendritic processes, which can vary according to the type of bone, *i.e.*, rounder in trabecular bone and elongated in cortical bone [16]. These cells are relatively inactive but can produce the components necessary to maintain the bone matrix. Moreover, the osteocytes retain their connections with adjacent osteocytes and are responsible for transducing the mechanical and chemical signals that guide bone remodeling. Therefore, osteocytes play an important role in controlling bone formation, resorption, and mineral homeostasis [19, 31, 32].

1.2.3.4 Osteoclasts

Osteoclasts are large and multinucleated cells that are involved in bone resorption [16, 33]. These cells derive from the hematopoietic stem cell lineage, particularly from the monocyte-macrophage precursors, and can be found in small pits at the bone's surface or

in regions of old and injured bone tissue. The osteoclasts characteristically present a ruffled border in the basal membrane's side, through which hydrochloric acid and proteases, such as cathepsin K, are released during the bone resorption [16, 34] Apart from their role in bone remodeling, osteoclasts can also regulate hematopoietic cells differentiation and produce factors such as clastokines that control osteoblasts during the bone remodeling cycle [16].

1.4 Bone regeneration process

The healing process of bone fractures is highly complex and involves the coordinated action of different cells and the expression of bioactive molecules to promote the resorption of the injured tissue and replace it with new tissue [35]. This cascade of events occurs when there is a bone lesion due to mechanical damage or derived from diseases such as osteoporosis, osteomyelitis, and osteoarthritis. The bone repair process is fundamental for restoring the bone's structure and function, both the mechanical and biological properties. Bone regeneration can be divided into two categories, primary healing (direct) and secondary healing (indirect), depending on the type of fracture [36].

1.4.1 Primary (direct) bone healing

Primary healing is characterized by bone regeneration without forming a periosteal or endosteal callus. This healing process is uncommon and occurs when there is an inexistent or short gap between the fracture ends, such is usually achieved via the establishment of rigid internal fixations. Such promotes the alignment of the fracture extremities and avoids/minimizes interfragmentary movement. When these conditions are achieved, primary healing can occur by direct remodeling of the lamellar bone, Havers canals, and blood vessels [37, 38].

Direct healing can occur through contact healing or gap healing, depending on the proximity of the fracture ends. Contact healing occurs when the space between bone ends is inferior to 0.01 mm and the interfragmentary tension is less than 2 % [39]. During this process, the bone matrix is produced by osteoblasts, and simultaneously occur the bone union and the restoration of the Havers system in the axial direction. This event allows the infiltration of blood vessels that contain osteoclastic precursors. Subsequently, the regenerated tissue is

remodeled into lamellar bone, finalizing the healing process without the development of periosteal callus [38].

Gap healing can be observed when the distance between the fracture ends is less than 800 μm – 1 mm [40]. In this healing process, the bone union and remodeling of Haversian canals are achieved at different time point. Initially, the fracture site is filled with lamellar bone that is mechanically weak but confers stability to the fracture joining the fracture ends. Afterward, the lamellar bone is remodeled longitudinally, *i.e.,* Havers system and osteons remodeling, restoring the native anatomical and biomechanical properties of the bone. This type of healing can take months to a few years for a complete healing to occur [38].

1.4.2 Secondary (indirect) bone healing

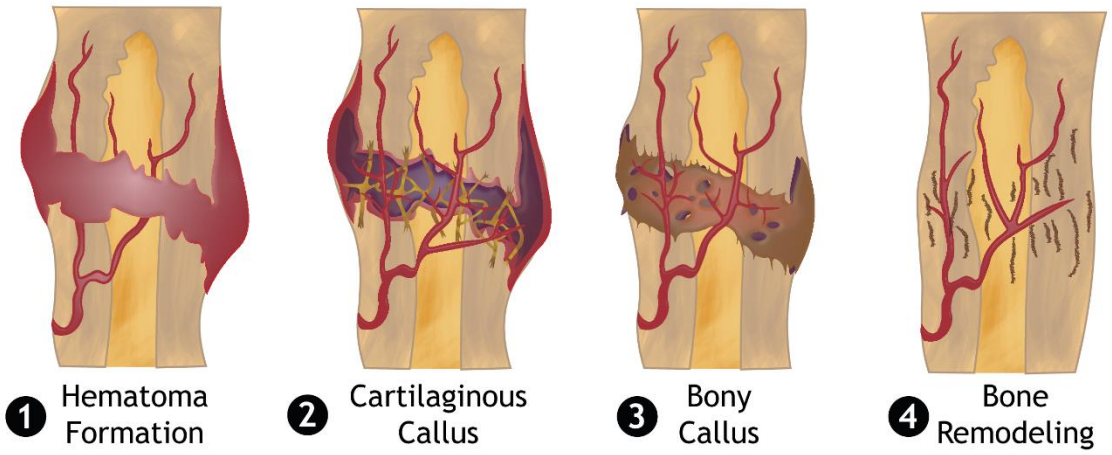

Figure 3. Illustration of the typical indirect healing phases.

Indirect healing is the most common form of fracture healing and it is divided into several phases, such as hematoma formation, cartilaginous callus, callus formation, and bone remodeling, (all these phases are depicted in Figure 3) [38].

After trauma occurs, a hematoma is formed containing peripheral and intramedullary blood cells, as well as bone marrow cells, to act as a mold for callus formation. This event induces a pro-inflammatory response, which involves the secretion of tumor necrosis factor-α (TNF-α), interleukin-1 (IL-1), IL-6, IL-11, and IL-18, that promote the recruitment of inflammatory cells and angiogenesis [41]. Along with osteoclasts, the inflammatory cells will mediate the removal of the damaged and necrotic tissue. Additionally, MSCs are recruited from surrounding soft tissues and bone marrow. At the bone lesion site, the MSCs

proliferate and differentiate into osteogenic cells, through the action of osteoinductive molecules (namely BMP-2 and BMP-7) [38, 42].

After primary hematoma formation, VEGF release leads to angiogenesis, and within the hematoma, fibrin-rich granulation tissue will start to be formed. At this point, MSC are recruited and begin to differentiate into fibroblasts, chondroblasts, and osteoblasts. This triggers the onset of chondrogenesis, where a collagen-rich fibrocartilaginous network covers the fracture's exterior and is surrounded by a sleeve of hyaline cartilage, that will stabilize the bone lesion. Simultaneously, osteoprogenitor cells deposit a layer of bone tissue, in the layers adjacent to the periosteum [43, 44].

Following this, endochondral ossification of the cartilaginous callus will start. During this process, the differentiation of chondroblasts and chondroclasts in osteoblasts and osteoclasts is stimulated by the expression of the receptor activator of nuclear factor kappa-β ligand (RANKL). This event will result in the resorption and calcification of the cartilaginous callus. The continuous angiogenesis supports the migration of MSC that will further support the regeneration process [43, 45]. After the formation of the hard callus, *i.e.*, immature bone, this tissue will undergo repeated remodeling due to the continuous migration of osteoblasts and osteoclasts. The osteoclasts will promote the bone matrix resorption whereas the osteoblasts form the new bone. Over time, the center of the callus is replaced by compact bone, while its edges are replaced by lamellar bone. This lengthy remodeling process results in the restoration of the native bone structure [43].

1.5 Bone Grafts

Bone grafting is one of the most explored surgical procedures to repair bone defects. The bone grafts can be classified as autografts, allografts, and xenografts according to the origin [44, 46]. Autografts consist of bone material harvested from one anatomical site and transplanted elsewhere within the same individual. Autografts present osteoconductive, osteoinductive, and osteogenic properties and are considered the gold standard, since they can be placed on the patient without causing many side effects. However, the limited availability, the pain, the increased blood loss and surgery duration, as well as the potential for the establishment of infections at the donor site, are some of the risks associated with this therapeutic approach [44].

Allografts are bone grafts harvested from one individual and transplanted into another individual of the same species. Considering the limitations of autografts, allografts arise as the next best alternative and are used in patients with low healing potential and pseudoarthrosis. However, allografts are immunogenic and may allow viral transmission between individuals, and the establishment of infections. Moreover, allografts also present limited osteoinduction and reduced mechanical strength due to sterilization by gamma irradiation [46].

Xenografts are grafts which the bone tissue is harvested from a different species. Despite the higher availability, xenografts are highly immunogenic, and can lead to interspecies disease transmission (*e.g.*, prions and retroviruses), as well as often present a of lack viable cells and biological components due to the tissue processing methods [47].

Considering the several disadvantages presented by bone grafts, in recent years, the researchers from bone tissue engineering field have been highly active developing a variety of bone substitutes, such as bone implants, injectable cement, scaffolds, and hydrogels. These engineered structures aim to mimic the structure of native bone and provide a suitable microenvironment for the bone regeneration process [8, 37].

1.6 Tissue Engineering

Tissue engineering (TE) is an emerging interdisciplinary field aiming to develop solutions capable of substituting or restoring the structure and function of native tissues by applying the principles of engineering and life sciences [48, 49]. In particular, Bone Tissue Engineering (BTE) focuses on the application of Top-Down or Bottom-Up approaches to create personalized three-dimensional (3D) structures with the ability to substitute the damaged bone or support their complete regeneration [50].

BTE solutions can be produced through the synergic combination of biomaterials (natural and/or synthetic polymers, ceramics, and composites), cells, growth factors, or other bioactive molecules that allow to mimic the native tissue and promote the re-establishment of the bone structure and functions [6, 51, 52]. Moreover, the bone substitutes/scaffolds must combine and match, as close as possible, both the physicochemical and biological properties of the native bone.

1.6.1 Properties exhibited by 3D scaffolds aimed for bone regeneration

Over the years, many studies have been conducted to produce an ideal structure for being applied to bone lesions as permanent or temporary replacements. Particularly, the application of scaffolds as temporary 3D structures that provide mechanical stability to the bone defect, while stimulating the migration, attachment, and proliferation of osteoinductive cells, necessary to the formation and restoration of new bone tissue is highly challenging [2, 53]. Moreover, the 3D scaffolds must also present a degradation profile that is similar to the rate of new bone formation [54]. In the following topics, the different properties essential for 3D scaffolds' application in bone regeneration are summarized, discussing their contribution to each step of this complex process.

1.6.1.1 Biocompatibility

Biocompatibility known as the capacity of a material/scaffold to perform its function (*e.g.*, promote cell adhesion, proliferation, and differentiation) without eliciting adverse local or systemic responses in the body (*e.g.*, immunogenic reaction, inflammation, and cell death) [55]. The scaffolds' biocompatibility is determined by several factors, such as the chemical composition, structure and surface morphology used. Furthermore, since scaffolds are often designed to act as temporary matrices, the products resulting from their degradation must be also biocompatible and ideally eliminated from the body without causing toxic side effects to the body [56].

1.6.1.2 Biodegradability

Biodegradability refers to the material/scaffold degradation profile (*i.e.,* breakdown into simpler substances such as water, basic elements, or smaller units) in the human body [57]. As previously referred, the bone scaffolds design must also consider the degradation profile and growth rate of the new tissue. In optimal conditions, the scaffold must be completely degraded when the damaged tissue is fully regenerated. The scaffolds' degradation usually occurs due to the cleavage of chemical bonds in the polymer chains, which leads to a decrease in their molecular weight. Additionally, the materials used in the bone scaffolds can also be reabsorbed and incorporated into the new bone tissue [56, 58].

1.6.1.3 Surface properties, osteoconductivity, and osteoinductivity

Scaffold-cell interactions depend on the surface properties of the biomaterials, namely charge, chemical composition, roughness, stiffness, and hydrophilic/hydrophobic character. These properties directly influence the cells' adhesion and proliferation processes [59]. Considering this, in bone tissue regeneration there are two biological properties considered fundamental for the scaffolds fully re-establish the structure and features of native bone, osteoconductivity and osteoinductivity. Osteoconductivity refers to the scaffolds' ability to support the attachment of osteoblasts or osteoprogenitor cells, as well as provide an interconnected structure that favors cell migration and angiogenesis processes [60, 61]. Osteoconductivity refers to the ability of scaffolds to promote the differentiation of osteoprogenitor cells into osteoblasts. Several findings have shown that rough and positively charged surfaces promote osteoconduction, as they create a matrix that favors cell adhesion and proliferation [62]. In addition, scaffolds may also be formulated to contain osteoinductive agents (*e.g.*, growth factors and/or bioactive molecules) that will induce the differentiation of bone cells [62].

1.6.1.4 Mechanical properties

Bone scaffolds are designed to act as permanent tissue replacements or as a temporary matrix that provides structural support until the complete bone restoration. Thus, scaffolds must display mechanical properties that mimic those found in native bone, namely the strength and stiffness [55]. Depending on the type of bone, *i.e.*, cortical and cancellous bone, the mechanical properties exhibited are different. The Young's modulus (elasticity, rigidity of a material) of cortical bone varies from 7 – 30 GPa, while that of cancellous bone ranges from 50 – 2000 MPa [60, 63-66]. On the other side, the compressive strength (the ability of a certain material to withstand loads values exhibited) by both cortical and cancellous bone ranges from 100 – 200 MPa, and 1 – 30 MPa, respectively [60, 63-66]. Therefore, the scaffolds must be developed considering the mechanical requirements of the injured bone.

1.6.1.5 Porosity

The porosity refers to the ratio between the volume of the pores and the overall scaffold volume. In this way, an ideal scaffold should present a porosity similar to that exhibited by trabecular bone (50 – 90 %) to allow cell penetration and differentiation as well as the

regeneration of damaged tissue [67]. Moreover, the pore size also impacts the scaffolds' performance. In the literature, the range of 100 – 300 μm of pore size is considered ideal to allow the exchange of essential nutrients, oxygen, and cellular metabolites, as well as cell migration [60, 67]. Furthermore, the presence of interconnected pores further facilitates the contact of fluids and cells with the interior regions of the scaffolds. Therefore, the overall porosity, pore size, and pore interconnectivity are crucial for the maintenance of cell viability and promotion of bone regeneration [60, 62]. Otherwise, the porous structure of the scaffolds also impacts significantly their mechanical behavior. In fact, highly porous scaffolds are known to exhibit low mechanical resistance and a higher rate of degradation [62]. Therefore, the researchers must consider the impact of the pore structure in the scaffolds' performance, principally finding a balance between the scaffolds' mechanical and biological properties [68].

1.6.1.6 Antibacterial activity

The establishment of bacterial infections is one of the main risks associated with the implantation of bone scaffolds [69]. The implanted scaffolds can be initially colonized by bacteria and develop the more dangerous biofilms, which are more resistant to antibacterial treatments and can maintain a persistent infection in the host [70]. For that purpose, the BTE solutions often possess in their structure antibacterial agents such as metal nanoparticles, antibiotics, and antimicrobial polymers to avoid bacterial adhesion or even induce the microorganisms' death [71].

1.6.2 Techniques used for scaffold fabrication

The scaffolds' production methods can be grouped into two main categories: conventional (*e.g.*, salt leaching, gas foaming, phase separation, vapor deposition, and freeze-drying) and rapid prototyping (RP) (*e.g.*, fused deposition modeling, selective laser sintering, and stereolithography) techniques [72, 73]. The conventional methods lack the precise control over the internal architecture of the scaffolds and/or are not compatible with the fabrication of scaffolds with complex geometries. In turn, the RP emerged in the last years as a highly promising production technique for developing BTE solutions. These technologies allow the fast production of scaffolds with a well-defined structure, *i.e.*, designed specifically to the patient lesion, and high reproducibility [74, 75]. The production of scaffolds by RP technologies can be divided in three main steps: i) scaffold model design in a 3D

computer-aided design (CAD) software (*e.g.*, SolidWorks®); ii) model processing for the production phase (*e.g.*, layer-by-layer conversion); iii) model printing. Furthermore, the utilization of RP technique in BTE is also compatible with both Top-Down and Bottom-Up approaches. The Top-Down approach is based on the initial printing of the full-sized scaffold only using the structural biomaterials, followed by the addition of biological agents (*e.g.*, cells and growth factors) [76]. In this approach, the scaffolds provide physical support for cell adhesion and regulate cell proliferation, migration, and differentiation. In the Bottom-Up approach, the printing of the scaffolds comprises both the structural biomaterials and biological agents (*e.g.*, cells and growth factors). Such allows the creation of scaffolds containing living cells embedded in the structural matrix and the spatial control over the arrangement of the cells, similar to that observed in the *in vivo* tissues [77]. In this work, a Top-Down approach was chosen due to the compatibility with a wider range of materials, from ceramics to polymers, and the capacity to create mechanically stronger scaffolds.

1.6.2.1 Scaffold fabrication with a Fab@Home 3D Plotter

The Fab@Home printer is a viable, economical, and reproducible RP technology compatible with the production of 3D structures with complex and well-defined geometries as well as controlled internal architecture. This printer produces the 3D model using a layer-by-layer method and is compatible with the utilization of different structural biomaterials, such as polymers, ceramics, or composites [74]. Briefly, the 3D CAD file of the desired scaffold is loaded in the printer software and structural biomaterials are placed into a syringe. Then, the Fab@Home printer will promote the successive deposition of the material in different layers by extrusion to a platform. The successive deposition of the layers allows the control of the pore size and the scaffolds' morphology and overall porosity [78]. The printing accuracy is dependent on the viscosity of the structural biomaterials' solution loaded in the syringe as well as on the printer parameters such as dispensing pressure, pushout (early dispensing before the cartridge starts to move along the printing path), suck-back (defines how much the plunger withdraws at the end of the printing path to stop the extrusion process), nozzle diameter (determines the resolution of the printing process), deposition rate (determines the amount of material deposited for each millimeter of printing path), printing speed (the speed at which the cartridge moves along the printing path), path height (distance between consecutive layers) and path space (space between adjacent printing paths) [79, 80].

1.6.3 Biomaterials used for scaffold fabrication

So far, several biomaterials, such as ceramics and/or natural/synthetic polymers have been explored to create BTE solutions that can reproduce the biological, mechanical, and structural properties of the bone as a permanent substitute or temporary support for tissue regeneration [54, 55]. Considering the composite nature of bone, inorganic (*e.g.*, hydroxyapatite) and an organic (*e.g.*, type I collagen) phase, most strategies focus on reproducing this composition in order to enhance their bone regeneration capacity. With this in mind, several composite materials, namely combining ceramics and polymers have been developed to present both the osteoconductivity, strength, and stiffness of the ceramics and the bioactivity of the polymers [81, 82]. In the following topics are described some of the most commonly explored ceramics and natural/synthetic polymers.

1.6.3.1 Ceramics

Ceramics are inorganic biomaterials that generally exhibit chemical and structural similarity with the inorganic phase of native bone, thus conferring biocompatibility, bioactivity (osteoconductivity and osteoinductivity), and providing high mechanical rigidity to the scaffolds. The most explored ceramics in BTE are calcium phosphate ceramics, such as hydroxyapatite (HAp) and tricalcium phosphate (TCP) [17].

1.6.3.1.1 Tricalcium phosphate

TCP is frequently used in the production of scaffolds for bone regeneration due to its biocompatibility, biodegradability and osteoconductivity. The TCP crystals present a higher porosity than hydroxyapatite leading to a faster resorption rate [83]. Nonetheless, the individual use of TCP has some disadvantages, such as mechanical fragility and low fatigue resistance [84]. The TCP scaffolds present a mechanical strength that is compatible with the requirements of native bone [85]. TCP has the ability to induce mineralization of the surface, which is crucial for improving bone regeneration [86]. Jeong and co-workers used β-TCP in conjugation with gelatin to produce 3D scaffolds for mimicking the bone composition [87]. This approach allowed to combine the mechanical properties of TCP (compressive strength similar to trabecular bone) with the gelatin capacity to support and promote the cell adhesion. Similarly, Park and colleagues produced a β-TCP/silk fibroin 3D

scaffold for application in bone regeneration [88].The authors reported that the addition of β-TCP enhanced the osteoconductivity and the mechanical performance of the silk fibroin 3D structures [88].

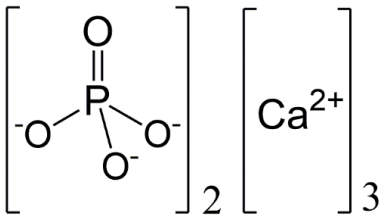

Figure 4. Chemical formula of tricalcium phosphate.

1.6.3.1.2 Hydroxyapatite

The HAp is the main ceramic component found in the bone and due to that it has been widely explored for producing BTE solutions [89] The HAp can stimulate the endogenous expression of osteogenic growth factors such as BMPs and increase the activity of alkaline phosphatase (ALP) in MCS [72]. However, this material is more expensive than TCP and also presents mechanical fragility (hard and brittle) that limits the applications of Hap ceramic scaffolds in load bearing sites [90]. Nosrati *et al.* fabricated a gelatin/HAp/graphene scaffold and observed that the addition of HAp (0.3 g) increased the mechanical properties of gelatin 3D structures from 0.062 – 0.26 MPa [91]. Moreover, Cox and colleagues 3D printed a HAp/poly(vinyl)alcohol scaffold with promising properties for osteoconduction and osteointegration [92].

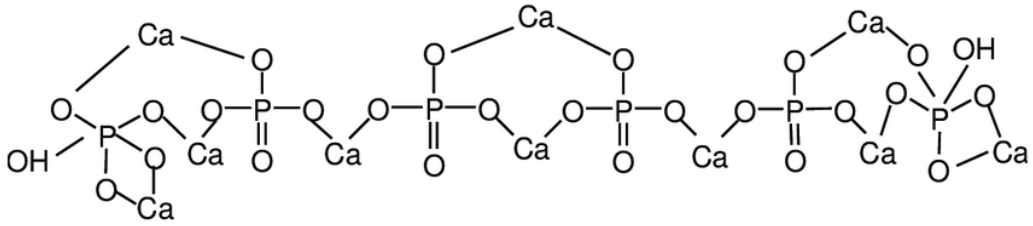

Figure 5. Chemical structure of hydroxyapatite.

1.6.3.2 Polymers

Polymers are macromolecules, that exhibit very advantageous properties for BTE application, such as biodegradability, biocompatibility, and bioactivity. According to their source, polymers can be classified as natural and synthetic.

1.6.3.2.1 Natural polymers

Natural polymers are obtained from natural sources, such as plants and animals, and are the predominant source of structural materials for TE applications due to their similarity with the native ECM [93]. Additionally, the natural polymers also present high biocompatibility and biodegradability as well as may contain cell-adhesion molecules. However, the natural polymers lack mechanical resistance for BTE application, present a fast degradation rate, are structurally more complex and the extraction process can be laborious, present batch variability, and represent a high cost [2, 17, 73]. Nevertheless, various natural polymers have already been investigated in bone tissue applications, namely proteins (collagen, fibrin, gelatin, silk fibrin), polysaccharides (hyaluronic acid, cellulose, starch, alginate, agarose, chitosan, and dextran) and phenyl-propane polymer (lignin) [17, 94].

1.6.3.2.1.1 Sodium Alginate

Sodium alginate (SA) is a natural polymer extracted from the cell walls of brown seaweed. SA is a linear anionic polysaccharide consisting of alternate blocks of 1,4-β-D-mannuronic (M) and α-L-guluronic (G) acids [95]. The SA is water soluble and can undergo ionotropic crosslinking in the presence of bivalent cations such as calcium (Ca^{2+}), strontium (Sr^{2+}), and barium (Br^{2+}) ions. Furthermore, SA is low cost, biodegradable, biocompatible, low immunogenic, mucoadhesive, pH-sensitive and have a high viscosity in contact with water [96, 97]. Wang and co-workers developed a silk fibroin/SA scaffold for TE applications [98]. The author reported that the scaffolds' polymeric structure resulted in highly porous structures that enhanced cell adhesion and proliferation. Furthermore, Oliveira *et al.* developed a SA 3D scaffold containing bioactive glass S53P4 utilizing a 3D printing technique [99]. The scaffolds production was dependent on the SA ionotropic gelation and resulted in biocompatible structures (*e.g.,* 100 % cell viability after 14 days), but presented sub-optimal mechanical performance for application in weight-bearing sites (*i.e.,* compressive strength of ≈ 5 MPa) [99].

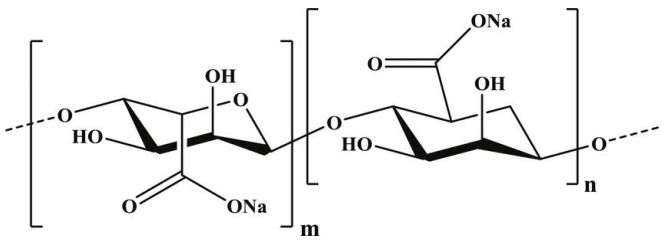

Figure 6. Chemical structure of sodium alginate.

1.6.3.2.1.2 Lignin

Lignin (LG) is one of the most abundant natural polymers, often found in the nature associated with cellulose microfibrils. LG has a complex, heterogeneous, and branched structure that originates from three phenyl-propane monolignols, such as coniferyl, sinapyl, and p-coumaryl [100]. However, LG can be extracted from different plant species such as grasses, dicots of angiosperms, and softwoods, which can lead to variations in their composition [101]. The LG is poorly soluble in water, biocompatible, and presents a high mechanical strength, which supports their application in BTE [102]. Despite the limited information available in the literature concerning the LG application in bone regeneration, research in TE field shows that the LG inclusion in hydrogels enhanced their mechanical properties and allowed the tuning of their wettability to values closer to that considered ideal for supporting the cell adhesion and proliferation [103, 104].

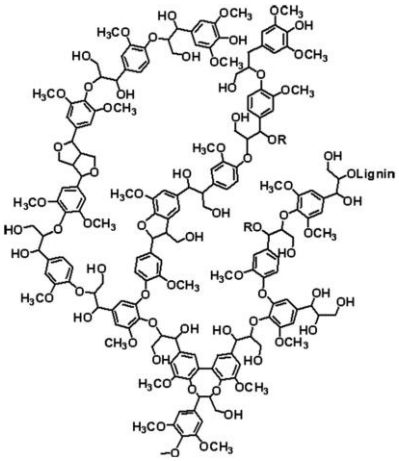

Figure 7. Chemical structure of lignin.

1.6.3.2.1.3 Collagen

Collagen is the most abundant protein in the ECM, maintaining their biological and structural integrity and providing physical support to the cells and tissues. Therefore, collagen is one of the preferential materials used for TE applications. It is characterized by its low immunogenicity, biocompatibility, biodegradability, and may also influence the cells morphology, adhesion, migration, and differentiation processes [105, 106]. Song and co-workers developed zinc silicate/nanohydroxyapatite/collagen 3D scaffolds and observed

that they could enhanced bone regeneration and angiogenesis *in vivo*, but presented low compressive strength (*i.e.*, inferior to 0.6 MPa) [107].

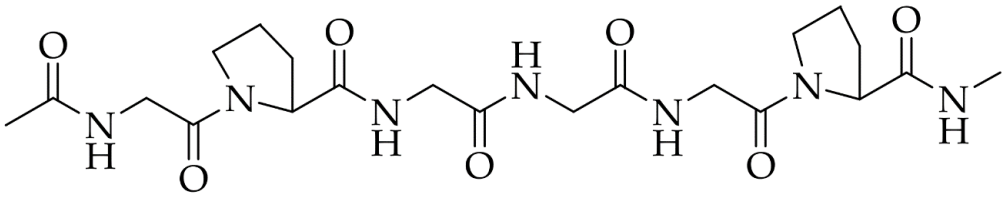

Figure 8. Chemical structure of collagen.

1.6.3.2.1.4 Chitosan

Chitosan is a cationic polysaccharide, obtained from the alkaline deacetylation of chitin, and formed by *D*-glucosamine and *N*-acetyl-*D*-glucosamine units linked through β-1,4 glycosidic bonds. This polymer is used in TE because it is bioactive, biodegradable, bioadhesive, hemostatic, and displays antimicrobial activity [108, 109]. Serra and colleagues demonstrated that chitosan/gelatin/β-TCP scaffolds are bioactive and biocompatible and presented antimicrobial activity against *Staphylococcus aureus* [110]. Georgopoulou *et al.* developed 3D scaffolds based in the crosslinking of chitosan and gelatin for application in the bone regeneration [111]. Despite the poor mechanical properties, the scaffolds were able to the formation of extracellular matrix and the expansion of fibroblasts.[111].

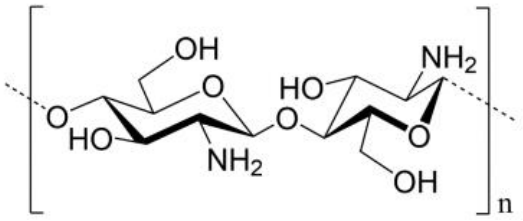

Figure 9. Chemical structure of chitosan.

1.6.3.2.2 Synthetic polymers

Synthetic polymers are produced artificially in laboratories and are used in BTE due to their chemical versatility, control over the degradation rate, excellent mechanical properties, and are cost-effective. Nevertheless, these polymers often present sub-optimal biological performances, such as lower biocompatibility and bioactivity. Aliphatic polyesters such as polylactic acid (PLA), polyglycolic acid (PGA), poly(acid-co- lactic acid) (PLGA), and poly(caprolactone) (PCL) are some of the most used synthetic polymers in BTE [2, 112].

1.6.3.2.2.1 Poly(caprolactone)

PCL is an aliphatic semi-crystalline, biocompatible, chemically and thermally stable polymer. Moreover, the PCL also present good mechanical properties that favor its application in TE. However, PCL has a low degradation rate and its hydrophobic nature difficult the cell adhesion and proliferation [73, 113, 114]. Zimmerling and co-workers showed the fabrication of PCL/nano-HAp 3D scaffolds for application in BTE using RP conjugated with four preparation techniques, melt-blending, powder blending, liquid solvent, and solid solvent techniques [115]. Fazeli *et al.* also produced PCL/HAp 3D scaffolds enriched with bioglasses for application in the bone regeneration [116]. The authors observed that the coating of PCL scaffolds with HAp and bioglasses improved the proliferation and osteogenic differentiation of stem cells. Moreover, the PCL/HAp 3D scaffolds showed an increase in the yield stress from 0.378 – 1.320 MPa [116].

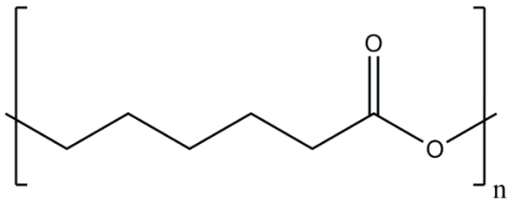

Figure 10. Chemical structure of poly(caprolactone).

1.7 Aims

The overall aim of the present thesis was to produce and characterize a new 3D scaffold functionalized with lignin for bone tissue regeneration applications.

The specific objectives of this study were:

- Optimization of the composition of the ceramic-polymer blend (TCP, SA, LG) to be used in scaffold's production;
- Production of TCP/SA and TCP/LG/SA scaffolds;
- Evaluation of the mechanical, physicochemical, and biological properties of the produced scaffolds.

Chapter 2

Materials and Methods

2. Materials and Methods

2.1 Materials

Alizarin Red S (ARS), Alkaline Phosphatase, Dulbecco's modified Eagle's medium (DMEM-F12), ethylenediaminetetraacetic acid (EDTA), diethanolamine, glutaraldehyde 2.5 % (v/v), hydrochloric acid (HCl), alkali lignin, phosphate buffered saline solution (PBS), di-Potassium hydrogen phosphate trihydrate ($HK_2O_4P.3H_2O$), resazurin, sodium alginate, sodium hydroxide (NaOH), and trypsin were purchased from Sigma-Aldrich (Sintra, Portugal). Normal human osteoblast (hOB; 406-05f) cells were bought from Cell Applications, Inc. (San Diego, USA). Fetal bovine serum was provided by Biochrom AG (Berlin, Germany). Calcium chloride ($CaCl_2$), sodium chloride (NaCl), Tris-buffered saline (TBS), and L-Ascorbic acid (LAA) were obtained from Fisher Scientific (Porto Salvo, Portugal). Tricalcium phosphate (TCP) was purchased from Panreac (Barcelona, Spain). Sodium bicarbonate ($NaHCO_3$) was obtained from Labchem (Santo Antão do Tojal, Portugal). Magnesium chloride hexahydrate ($MgCl_2.6H_2O$), potassium chloride (KCl), and sodium sulfate anhydrous (Na_2SO_4) were purchased from Labkem (Barcelona, Spain). Ethanol 99.5 % (EtOH) was obtained from Aga (Prior Velho, Portugal). Double deionized and filtered water was obtained using a Milli-Q Advantage A10 ultrapure Water Purification System (0.22 μm filtered; 18.2 MΩ/cm at 25 ˚C).

2.2 Methods

2.2.1 Production of scaffolds

The different formulations of the 3D scaffolds were prepared by varying the LG/SA ratio, according to Table 1. For that purpose, the SA and LG were sequentially dissolved in double deionized and filtered water and homogenized using an X10/25 Ultra-turrax for 35 min. Subsequently, the TCP content was added to the polymeric mixture and homogenized for 20 min. The prepared TCP/LG/SA mixture was then loaded into a syringe (10cc Luer Lock) and extruded using the Fab@Home 3D printer, originating the 3D TCP/LG/SA scaffolds. After the printing process, the scaffolds were immersed in a 5 % $CaCl_2$ (w/v) solution for 24 h to achieve the full crosslinking of the SA chains, both in the scaffolds' exterior and interior. Afterward, the scaffolds were removed from the $CaCl_2$ solution and dried at 37 ˚C for 3 days.

Table 1. Summary of the produced scaffolds and their composition.

	Scaffolds			
	TCP/LG/SA			**TCP/SA**
	1:3	**1:2**	**1:1**	
LG/SA ratio	1:3	1:2	1:1	-
TCP (g)	6	6	6	6
SA (g)	1.125	1	0.75	1.5
LG (g)	0.375	0.5	0.75	-
Density (g/mL)	0.75			

2.2.2 Characterization of the morphology of the 3D scaffolds

The scaffolds' morphology, surface, and macroporosity were characterized using Scanning Electron Microscopy (SEM). For this purpose, the samples were mounted on aluminum stubs, using araldite glue, and coated with gold, using a Quorum Q150RES sputter coater (Quorum Technologies, UK). Then the scaffolds' images at different magnifications were acquired in a Hitachi S-3400N scanning electron microscope (Japan) operated at an accelerating voltage of 20 kV.

2.2.3 Characterization of the scaffolds' physicochemical

2.2.3.1 Attenuated Total Reflectance- Fourier Transform Infrared spectroscopy

Attenuated Total Reflectance Fourier Transform Infrared (ATR-FTIR) spectroscopy was used to characterize the chemical composition of the scaffolds. Spectra were acquired with an average of 128 scans, with a spectral resolution of 32 cm^{-1} and a range of 400 – 4000 cm^{-1} [117]. The scaffolds were crushed into powder and then mounted on a diamond window in order to allow the samples' analysis using the Nicolet iS10 FTIR Spectrophotometer (Thermo Scientific, Waltham, MA, USA). For comparison purposes, all the raw materials used in the production of the scaffolds were analyzed in their pure state.

2.2.3.2 Energy dispersive spectroscopic analysis

Energy Dispersive Spectroscopy (EDS) was used to determine the elemental composition of the 3D scaffolds. Briefly, the samples were placed on aluminum stubs, air-dried at room temperature (RT), and then analyzed in an XFlash Detector 5010 (Bruker Nano, Germany).

2.2.4 Characterization of the scaffolds' mechanical properties

The mechanical properties of the scaffolds (n=5) were analyzed in dry and wet conditions, to also mimic the physiological environment found *in vivo*. The wet scaffolds were immersed overnight in the standard simulated body fluid (SBF). The SBF solution has almost identical ion concentrations as the human blood plasma (142.0 mM Na^+, 5 mM K^+, 1.5 mM Mg^{2+}, 2.5 mM Ca^{2+}, 147.8 mM Cl^-, 4.2 mM HCO_3^-, 1.0 mM HPO_4^{2-} and 0.5 mM SO_4^{2-}) at a pH of 7.4. This solution was prepared using a method previously described in the literature [118].

Then, the samples were subjected to compression tests to evaluate the mechanical behaviour of the scaffolds. The samples' testing was performed at RT using a Shimadzu AG-X tensile testing machine (Tokyo, Japan) with a load cell of 5 kN and a cruising speed of 2 mm/min.

The compressive strength (*Cs*) was calculated using Equation (1) [119]:

$$Cs = \frac{F}{w \times l} \qquad (1)$$

Where F represents the load at the time of fracture, w and l correspond to the width and length of the scaffolds, respectively.

Young's modulus (*YM*) was also calculated using the stress-strain relationship, shown in Equation (2) [119]:

$$YM = \frac{Cs}{H_d} \qquad (2)$$

Where *Cs* corresponds to the scaffold compressive strength and H_d symbolizes the height deformation at maximum load.

2.2.5 Characterization of the scaffolds' swelling profile

The scaffolds' swelling capacity was evaluated using a method previously described in the literature [120]. Briefly, scaffolds (n=5) were immersed in Tris-buffered saline (TBS) (1x, pH 7.4) and incubated under stirring (60 rpm) at 37 ˚C for ≈ 3 days. At predetermined intervals, scaffolds were removed from the solution, weighed, and re-immersed in the solution. The swelling ratio was then calculated using Equation (3):

$$Swelling\ Ratio\ (\%) = \left(\frac{W_t - W_o}{W_o}\right) \times 100 \qquad (3)$$

Where W_t indicates the final weight of the scaffolds, and W_o refers to the initial weight.

2.2.6 Contact angle measurements

The scaffolds' hydrophilicity was characterized using the sessile drop method of water contact angle (WCA) measurement. For that purpose, a drop of deionized water (10 uL) was automatically dispersed onto the sample's surface and the resultant contact angle was assessed using a Dataphysics OCA 20 contact angle analyzer (Dataphysics Instruments, Filderstadt, Germany). Ten measurements on several points of the scaffolds' surface were performed in order to determine the mean static contact angle and its standard error.

2.2.7 Evaluation of scaffolds' porosity

The total porosity of the scaffolds was evaluated using a liquid displacement method, as previously described [121]. Initially, the scaffolds were weighed and then immersed in absolute ethanol (EtOH) for 48 h. After this period, the samples were weighed again. EtOH was chosen because of its ability to penetrate the structure of the scaffolds without generating structural changes, *i.e.*, swelling or shrinkage [122]. The scaffolds' porosity was calculated using the Equation (4):

$$Porosity\ (\%) = \frac{W_w - W_d}{D_{EtOH} \times V_{scaffold}} \times 100 \qquad (4)$$

Where W_w and W_d correspond to the final and initial scaffold's weight of the scaffold, respectively. D_{EtOH} refers to the EtOH density at RT and the $V_{scaffold}$ corresponds to the scaffolds' volume.

2.2.8 Analysis of the biodegradation profile of the scaffolds

The scaffolds' degradation profile was evaluated in the absence or presence of lysozyme. For that purpose, the scaffolds were incubated in DMEM-F12 medium (with or without lysozyme), at 37 ˚C, under agitation (60 rpm) [79, 123]. At predetermined intervals, the scaffolds were removed from the solution, frozen at -80 ˚C, freeze-dried for 3 h, and weighted. The weight loss percentage at each timepoint was determined using Equation (5):

$$Weight\ loss\ (\%) = \left(\frac{W_i - W_f}{W_i}\right) \times 100 \qquad (5)$$

Where W_i refer to the initial weight of the scaffold and W_f represents the weight of the scaffolds at time t.

2.2.9 Characterization of the scaffolds' biological properties

2.2.9.1 Evaluation of the scaffolds' effect on the viability and proliferation of hOB cells

The scaffolds' cytotoxic profile was evaluated on hOB cells using the resazurin assay [123]. Initially, the different scaffold formulations were cut into small pieces, deposited in 96-well plates, and sterilized by ultraviolet radiation for 1 h. Subsequently, 10×10^3 cells/well were seeded in contact with the samples and incubated for 1, 3, and 7 days. At the predetermined times, the medium was removed, and the cells were incubated with 110 µL of fresh medium containing resazurin (10 µL) for 4 h in the dark (37 ˚C, 5 % CO_2). Then, the resorufin fluorescence was measured (λ_{ex} = 560 nm and λ_{em} = 590 nm) using Spectramax Gemini EM spectrofluorometer (Molecular Devices LLC, CA, USA). Cells incubated without materials and cells incubated with EtOH (70 %) were used as negative (K^-) and positive (K^+) controls, respectively.

2.2.9.2 Characterization of cell adhesion at the surface of the scaffolds

SEM was used to evaluate the cell adhesion on the surface of the scaffolds. For this purpose, hOB cells were seeded on the scaffolds and incubated for 1, 3, and 7 days. After, in the predetermined timepoints, the scaffolds were fixed with glutaraldehyde (2.5 % (v/v)) for 30 min. Subsequently, the samples were frozen at -80 ˚C, freeze-dried for 3 h, and finally analyzed by SEM analysis (as described in Section 2.2.2).

2.2.9.3 Evaluation *in vitro* biomineralization

The bioactivity of the scaffolds was evaluated upon immersion in SBF solution (prepared as described in Section 2.2.4.) and incubated at 37 °C for 7 and 21 days [118]. At the predetermined intervals, the scaffolds were removed from the SBF solution and dried to analyze the deposition of calcium and phosphate ions and also to verify the presence of apatite layers, using SEM.

Alizarin Red S (ARS) staining was also performed to study the scaffolds' ability to stimulate calcium deposition by hOB cells, using a previously optimized protocol [124]. Briefly, hOB cells were grown for 1, 3, 7, and 14 days in the presence of the scaffolds. Afterward, samples were fixed with formaldehyde (4 % (v/v)) for 1 h and stained with ARS (1 mL, 40 mM, pH=4.1 – 2.3). Then, the samples were washed with deionized water, to remove ARS excess, and the calcium deposition was quantified by measuring the ARS absorbance. For that purpose, samples were incubated under stirring with acetic acid (1 mL; 10 % (v/v)) for 30 min, vortexed for 30 s, and heated to 85 ˚C for 10 min. Subsequently, the samples were centrifuged (14 000 g, 25 min, RT) and the supernatant was neutralized with ammonium hydroxide (200 µL; 10 % (v/v)). Finally, the samples' absorption was read at 405 nm using a Biorad xMark microplate spectrophotometer. Additionally, a calibration curve for ARS was also performed for quantification purposes.

2.2.10 Statistical analysis

The acquired results were statistically analyzed using one-way analysis of variance (ANOVA) with the Newman-Keuls post hoc test. A p-value lower than 0.05 ($p < 0.05$) was considered statistically significant.

Chapter 3

Results and Discussion

3. Results and Discussion

3.1 Morphological characterization of the scaffolds

The 3D scaffolds were produced via the layer-by-layer deposition of the TCP, SA, and LG mixture using the Fab@Home 3D printer. The composition of the 3D printed mixture mimicked the natural bone matrix composition (20 – 30 % organic, 70 – 80 % inorganic) [79, 117]. The TCP was selected to mimic the inorganic phase, to confer the mechanical and osteogenic properties to the scaffolds. Otherwise, in the organic phase, SA was utilized due to its biocompatibility and biodegradability, whereas the LG further contributes to the mechanical properties. The macroscopic images (Figure 11 A) show that the introduction of LG induces changes in the 3D scaffolds' colour, from white to light brown, being darker in the TCP/LG/SA_1:1 scaffolds due to higher LG content. Nevertheless, all the formulations presented similar dimensions, designs, and shapes. Additionally, the scaffolds' surface morphology was further characterized by SEM (Figure 11 B). The SEM images show that the TCP/LG/SA and TCP/SA scaffolds present a similar irregular and rough surface. Such characteristics have been associated with enhanced bioactivity due to the higher number of anchorage points, which in turn can promote protein adsorption and cell adhesion. Moreover, literature data also show that rough and irregular surfaces can lead to higher production of extracellular matrix components as well as increase the metabolism of human osteoblast cells [125-127].

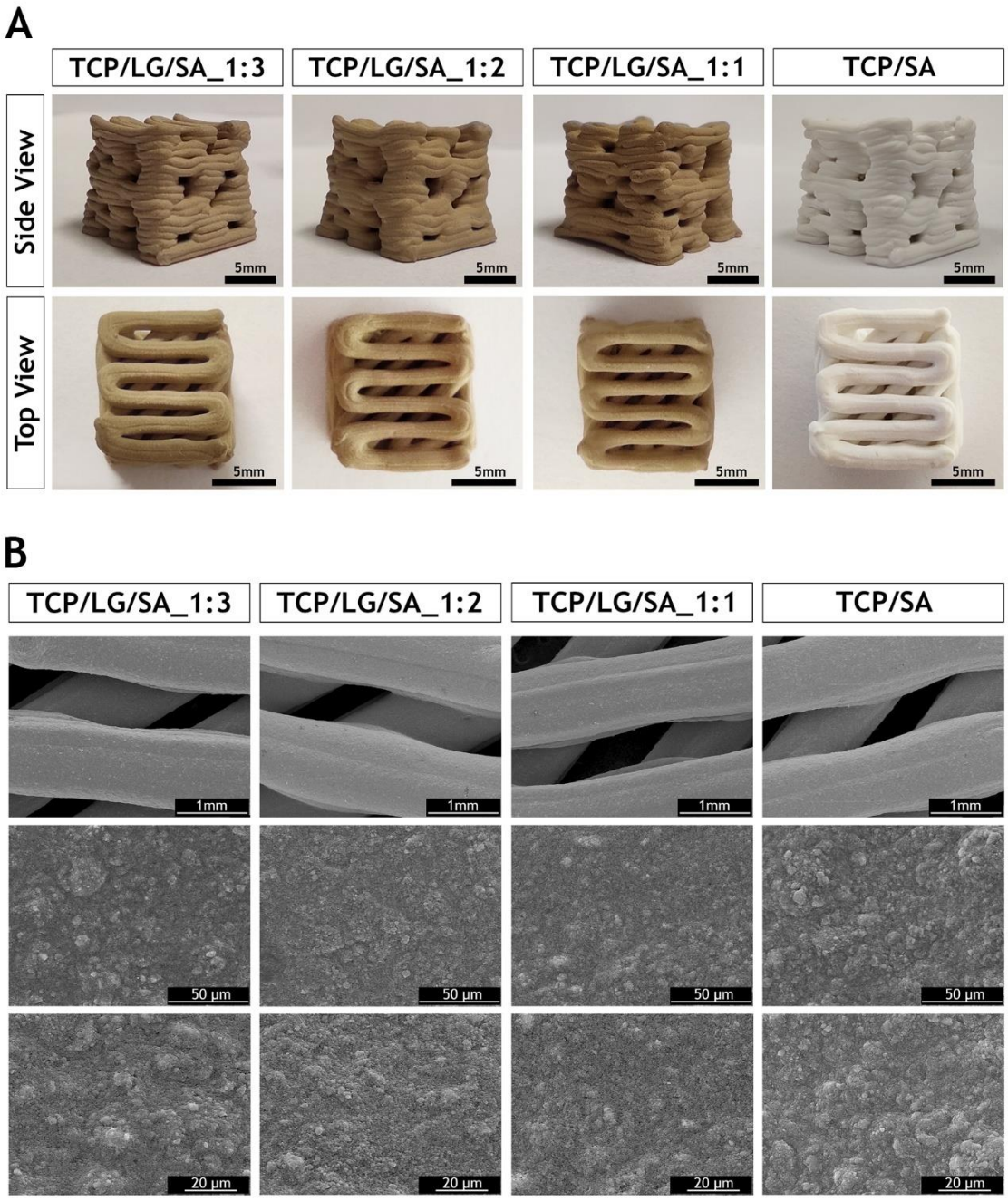

Figure 11. Production and characterization of 3D scaffolds. Representative macroscopic images of the different scaffolds produced (side and top views) (A) and SEM images showing the morphology and surface topography of the 3D scaffolds produced at different magnifications (B).

3.2 Characterization of the scaffolds' physicochemical properties

3.2.1 ATR-FTIR analysis

The chemical composition of the 3D scaffolds was analyzed by ATR-FTIR (Figure 12). The raw materials spectra show that the TCP exhibits a single characteristic peak at 1020 cm^{-1}, attributed to the P=O vibration. Moreover, in the SA spectra were identified two peaks at 1400 and 1600 cm^{-1}, corresponding to the C=O stretching of the carboxylate group, a band between 3000 – 3600 cm^{-1}, due to the OH groups of the alginate's G and M units, and vibration bands at 2930 – 2845 cm^{-1}, attributed to the C-H bonds. The LG's spectrum also shows a broad peak between 3000 – 3600 cm^{-1} that corresponds to OH groups and two peaks at 1131 and 1026 cm^{-1} attributed to the C-O bonds. Additionally, the LG also displays peaks at 2933 and 1583 cm^{-1} relating to the C-H and C=O stretch vibrations, respectively. Regarding the TCP/LG/SA and TCP/SA 3D scaffolds it is possible to observe the presence of the major peaks of each raw material. The TCP/SA shows the peaks at 3000 – 3600 cm^{-1}, 1131 – 1026 cm^{-1}, and 1020 cm^{-1} characteristics of TCP and SA materials, confirming the presence of raw materials in the scaffolds' composition. Similar data were obtained for TCP/LG/SA scaffolds, being observed the characteristic peaks for TCP, SA, and LG.

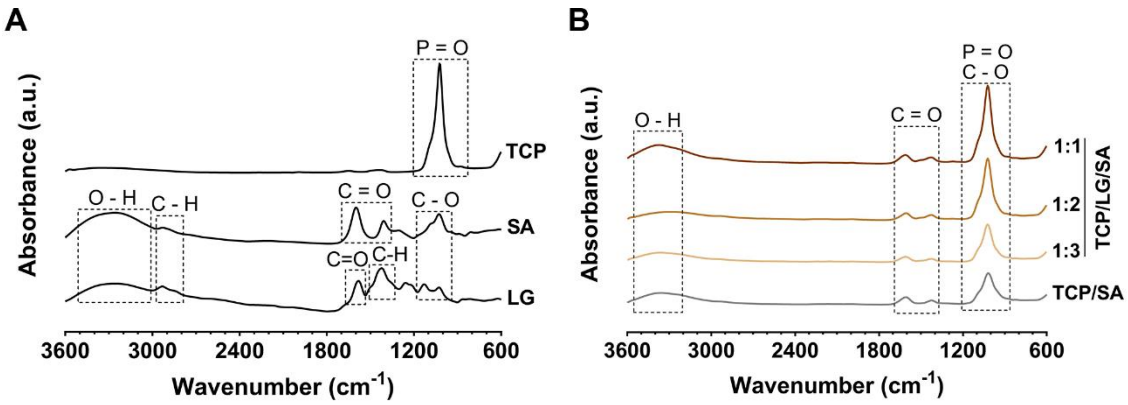

Figure 12. ATR-FTIR analysis of TCP, SA, LG (A) and TCP/LG/SA_1:3, TCP/LG/SA_1:2, TCP/LG/SA_1:1, and TCP/SA scaffolds (B).

3.2.2 Energy dispersive spectroscopy analysis

The scaffolds' composition was further characterized via EDS analysis (Table 2). Compared to the TCP/SA scaffolds, the TCP/LG/SA_1:2 and TCP/LG/SA_1:1 scaffolds demonstrated a higher content of carbon and a lower amount of oxygen elements (Table 2). While TCP/SA scaffolds compared to TCP/LG/SA_1:3 maintained a similar carbon and oxygen content. These differences can be explained by the higher LG content in the TCP/LG/SA_1:2 and TCP/LG/SA_1:1 scaffolds. Moreover, all formulations presented Ca/P ratios, in atomic % (Appendix I - Table C1), close to that observed in native trabecular bone, usually within the 1.3 – 2.2 range [128].

Table 2. EDS analysis of the 3D printed scaffolds.

	Elements ([a]wt.%)					
Sample	C	O	Na	P	Cl	Ca
TCP/LG/SA_1:3	11.64±4.57	45.86±14.09	0.16±0.09	8.97±0.88	2.99±0.3	30.37±2.17
TCP/LG/SA_1:2	13.47±4.71	43.58±12.37	0.17±0.09	9.06±0.82	3.16±0.29	30.57±2.01
TCP/LG/SA_1:1	16.04±5.53	46.03±13.29	0.16±0.08	8.81±0.83	2.52±0.25	26.44±1.80
TCP/SA	11.64±4.57	45.86±14.09	0.16±0.09	8.97±0.88	2.99±0.30	30.37±2.17

[a]wt.% - weight percentage

3.3 Characterization of the 3D scaffolds' mechanical properties

Scaffolds' mechanical stability is crucial for the bone regeneration process. Therefore, the scaffolds' mechanical properties are fundamental for their role in supporting the bone regeneration process, acting as temporary replacements that maintain or improve bone tissue functions [60, 85]. Moreover, the mechanical properties should be as close as possible to the bone tissue that needs replacement, for example, stiffer scaffolds can cause stress-shielding whereas lower stiffnesses fail in providing mechanical stability to the lesion [129]. Herein, the mechanical properties (*i.e.*, compressive strength (*Cs*) and Young's modulus (*YM*)) of TCP/LG/SA_1:3, TCP/LG/SA_1:2, and TCP/LG/SA_1:1 scaffolds were compared against TCP/SA scaffolds, both in dry and wet state (Figure 13). The obtained results show that the scaffolds have higher *Cs* and *YM* in dry conditions than in wet conditions. In a dry state, the TCP/LG/SA_1:3, TCP/LG/SA_1:2, TCP/LG/SA_1:1, and TCP/SA scaffolds presented a *Cs* of ≈ 20, 21, 13 and 18 MPa, respectively. Such data shows that the lignin introduction can lead to stiffer materials, revealing an increase of 15 % in

TCP/LG/SA_1:2 when compared to TCP/SA scaffolds. Moreover, the *Cs* values were within the upper range observed in native bone, 1 – 30 MPa. In turn, these values significantly decreased for all the tested formulations in the wet state, presenting a *Cs* of ≈ 1 MPa.

Similarly, the TCP/LG/SA_1:3, TCP/LG/SA_1:2, and TCP/SA scaffolds, in dry state, presented a *YM* value of ≈ 97, 96, 54 and 100 MPa, a value close to that observed in native trabecular bone (50 – 2000 MPa). Furthermore, in wet conditions, these values significantly decreased to ≈ 7 MPa. In fact, LG inclusion is further supported when compared with other works available in the literature. Boga and colleagues developed a TCP/alginic acid 3D scaffold (80/20 ratio) that presented increased brittleness, *Cs* of 8 MPa (Dry) and *YM* of 69 MPa (Dry) [123]. Moreover, Castilho *et al.* also described the production of TCP/alginate 3D scaffolds using a powder printing technique [130]. However, the produced scaffolds showed a maximum *Cs* of 20 MPa.

Altogether, these data show that the LG inclusion increases the mechanical resistance of the TCP/SA 3D scaffolds, nevertheless both *Cs* and *YM* values are still within the range of trabecular bone. In this way, the TCP/LG/SA scaffolds should be applied to lesions in low load-bearing bones.

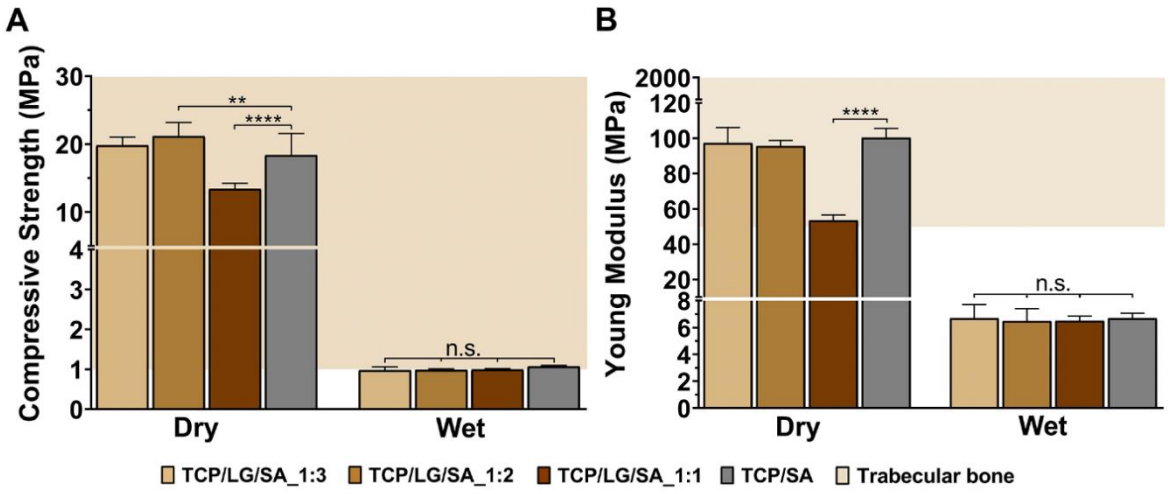

Figure 13. Characterization of the 3D scaffolds' Cs (A) and YM (B), under dry and wet conditions. Data are presented as mean ± standard deviation, n = 5, **p < 0.01 and ****p < 0.0001; n.s. – not statistically significant.

3.4 Evaluation of the 3D scaffolds' swelling profile

Scaffolds' swelling capacity is essential for their application in bone regeneration. The swelling can induce changes in the structure and size of the scaffolds, directly affecting their biological performance. For example, a high swelling capacity often results in the expansion

of the polymeric matrix, which can mediate the increase of the scaffolds' pore size and therefore facilitate the cells' penetration and adhesion as well as the diffusion of molecules along the scaffolds' structure. However, excessive swelling may induce the loss of the scaffolds' mechanical integrity and also induce compressive stress in the surrounding tissue [131].

The swelling of the 3D scaffolds was investigated by incubating in TBS solution, for ≈ 3 days (Figure 14 A). The four formulations exhibited a similar swelling profile, with a fast abrupt swelling in the first 7.50 h, followed by a plateau phase (Figure 14 A). However, the TCP/SA scaffolds showed a higher swelling ratio than TCP/LG/SA counterparts. These results are attributed to the higher content of hydrophilic SA in TCP/SA formulations. In turn, the TCP/LG/SA formulation with a higher amount of hydrophobic LG, the TCP/LG/SA_1:1, showed a lower swelling ratio during the experiment.

3.5 Determination of the 3D scaffolds' wettability

The scaffolds' wettability was evaluated by measuring the WCA at the materials' surface [132, 133]. The hydrophilicity can affect both protein adsorption and cell adhesion. In the literature, it is reported that cell adhesion is favoured on surfaces displaying a moderate hydrophilic character (40° < WCA < 70°), than on hydrophobic (WCA > 90°) or super hydrophilic surfaces (WCA < 20°) [134, 135].

The results revealed that scaffolds TCP/SA exhibit a WCA value of ≈ 13°, demonstrating a super hydrophilic character (Figure 14 B). However, highly hydrophilic surfaces limit or completely impair cellular attachment and spreading. In fact, cell adhesion mediating molecules interact weakly with super hydrophilic surfaces. In turn, the inclusion of the more hydrophobic LG changed the scaffolds' wettability, with a WCA value of ≈ 31° for TCP/LG/SA_1:3, ≈ 33° for TCP/LG/SA_1:2 and TCP/LG/SA_1:1 scaffolds (Figure 14 B). Therefore, the LG inclusion resulted in scaffolds with a wettability closer to that considered ideal for biological applications. Such results are in accordance with other works reported in the literature that included LG in the scaffolds formulation. Mohammadalipour *et al.* observed that the addition of LG to polyhydroxybutyrate electrospun scaffolds enhanced the observed wettability, resulting in scaffolds with a moderate hydrophilic character WCA of 73° [136].

3.6 Evaluation of scaffolds' porosity

Scaffolds' porosity (*i.e.*, overall porosity, pore size, and pore interconnectivity) has a remarkable effect on cells' infiltration, proliferation, and growth. The pore size is essential to modulate the cells' movement to the interior regions of the scaffolds. Moreover, the interconnected pores can also facilitate the diffusion of different agents throughout the scaffolds, such as the Ca^{2+} and PO_4^{3-} ions allowing the formation of a hydroxyapatite-like layer [137].

The total porosity of the scaffolds was measured using the liquid displacement method (Figure 14 C). All the formulations presented a total porosity of 37 – 41 %, slightly lower than the ideal for trabecular bone (50 – 90 %). However, it is worth noticing that highly porous scaffolds may present sub-optimal mechanical strength due to their lower density. Furthermore, SEM images showed a macroporosity (1650 ± 250 μm x 650 ± 150 μm) compatible with cells' infiltration, new vessels' ingrowth as well as for promoting an adequate exchange of nutrients and oxygen (Figure 14 D). Additionally, the obtained porosity values are similar to those observed in the literature for different ceramic/polymer compositions. For example, Boga and co-workers observed that the 3D printed TCP/alginic acid scaffolds at a ratio of 80/20, 70/30, and 60/40 presented an overall porosity of 50 %, 41 %, and 28 %, respectively [123]. Similarly, Diao *et al.* reported an overall porosity ranging from 38.25 to 63.78 % for 3D printed TCP scaffolds [138].

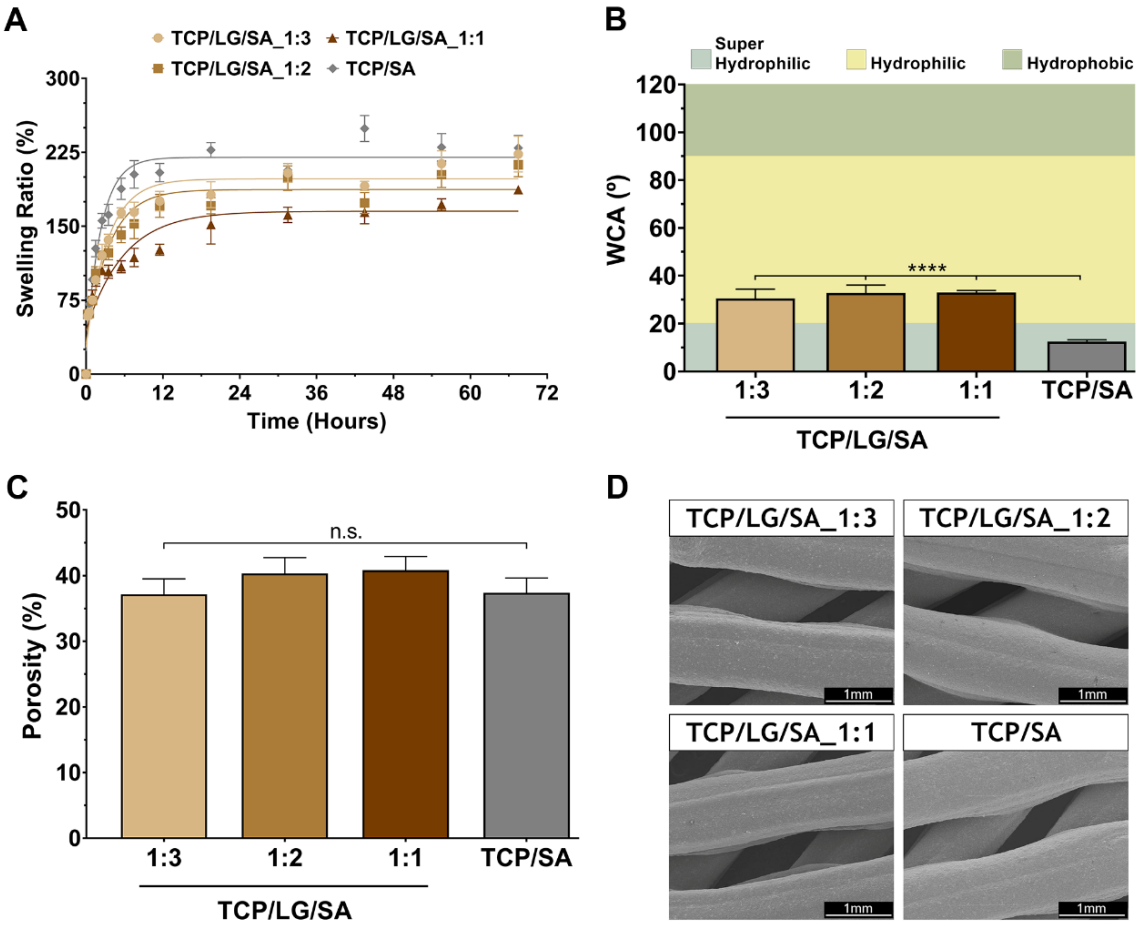

Figure 14. Characterization of the 3D scaffolds' physicochemical properties. Analysis of the scaffolds' swelling profile (A); evaluation of the scaffolds' surface wettability (B); characterization of the scaffolds' total porosity (C); representative SEM images of the scaffolds' macroporosity (D). Data are presented as mean ± standard deviation, n = 5, ****p < 0.0001; n.s. - not statistically significant.

3.7 Characterization of biodegradation profile of the scaffolds

The biodegradation profile is fundamental for assessing the application of 3D scaffolds as temporary supports for enhancing the bone regeneration process [62]. In this regard, scaffolds' degradation rate must be proportional to the rate of new bone formation, without compromising the stability of the construct or the integrity of the tissue at the injured site. For that purpose, the 3D scaffolds' degradation profile was evaluated in DMEM-F12 in the absence or presence of lysozyme, an enzyme found in saliva, granules of neutrophils, macrophages, and serum (Figure 15). The obtained results show that in the absence of lysozyme all formulations presented a maximum of ≈ 8 % weight loss, after 21 days. In the same period, in the presence of lysozyme, the total weight loss of the scaffolds increased to

≈ 12 %. Such can be justified by the lack of specificity of lysozyme towards SA and LG. In fact, the SA is mainly degraded *in vivo* by alginate lyases, whereas the LG can be slowly broken down by β-etherases [139, 140]. Cheng and colleagues also reported a slow degradation profile of PLGA/β-TCP 3D scaffolds, reaching a total weight loss of 2.2 % after 30 days [141]. In turn, Cabral and co-workers demonstrated that TCP/gelatin/chitosan scaffolds are degraded at a higher rate in the presence of lysozyme, which can degrade the chitosan, reaching a 20 % total weight loss after 20 days of incubation [124]. Therefore, the slower degradation profile observed for the TCP/LG/SA scaffolds can be explained by the lack of enzymes specific to LG and/or SA.

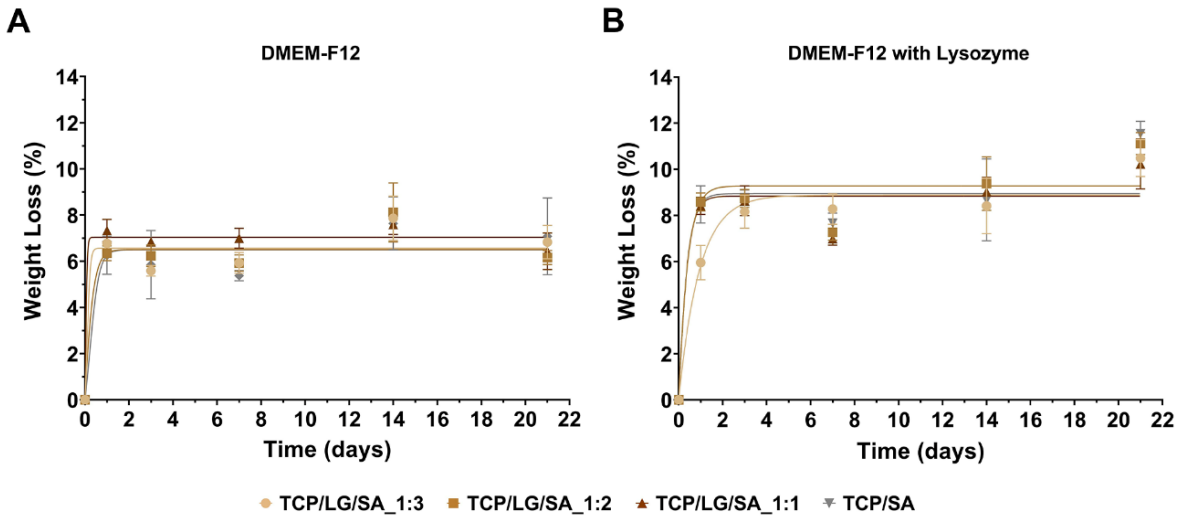

Figure 15. Evaluation of the 3D scaffolds' weight loss over time in the absence (A) or presence (B) of lysozyme. Results are presented as mean ± standard deviation, n=5.

3.8 Characterization of the biological properties of the produced scaffolds

3.8.1 Evaluation of scaffolds' cytotoxic profile

The cytotoxic profile of the produced scaffolds and their degradation products was evaluated on hOB cells using the resazurin assay. The optical microscopy images also show that hOB cells proliferate and exhibit a normal elongated and flattened morphology when in contact with all 3D scaffolds (Figure 16). Furthermore, the obtained results revealed that hOB cells remained viable when in contact with the scaffolds for 7 days (Figure 17 A). Otherwise, SEM analysis clearly shows the cells' adhesion and spreading at the surface of the scaffolds. Additionally, after 7 days, the increase in the cell density led to the establishment of several connecting points between cells and maintained the typical

osteoblastic morphology (Figure 17 B). Such data is in accordance with the safety profile described in the literature for materials based on TCP, SA, and LG or even their combination [79, 130, 136]. Therefore, the obtained results demonstrate that the LG addition does not compromise the biological application of these structures.

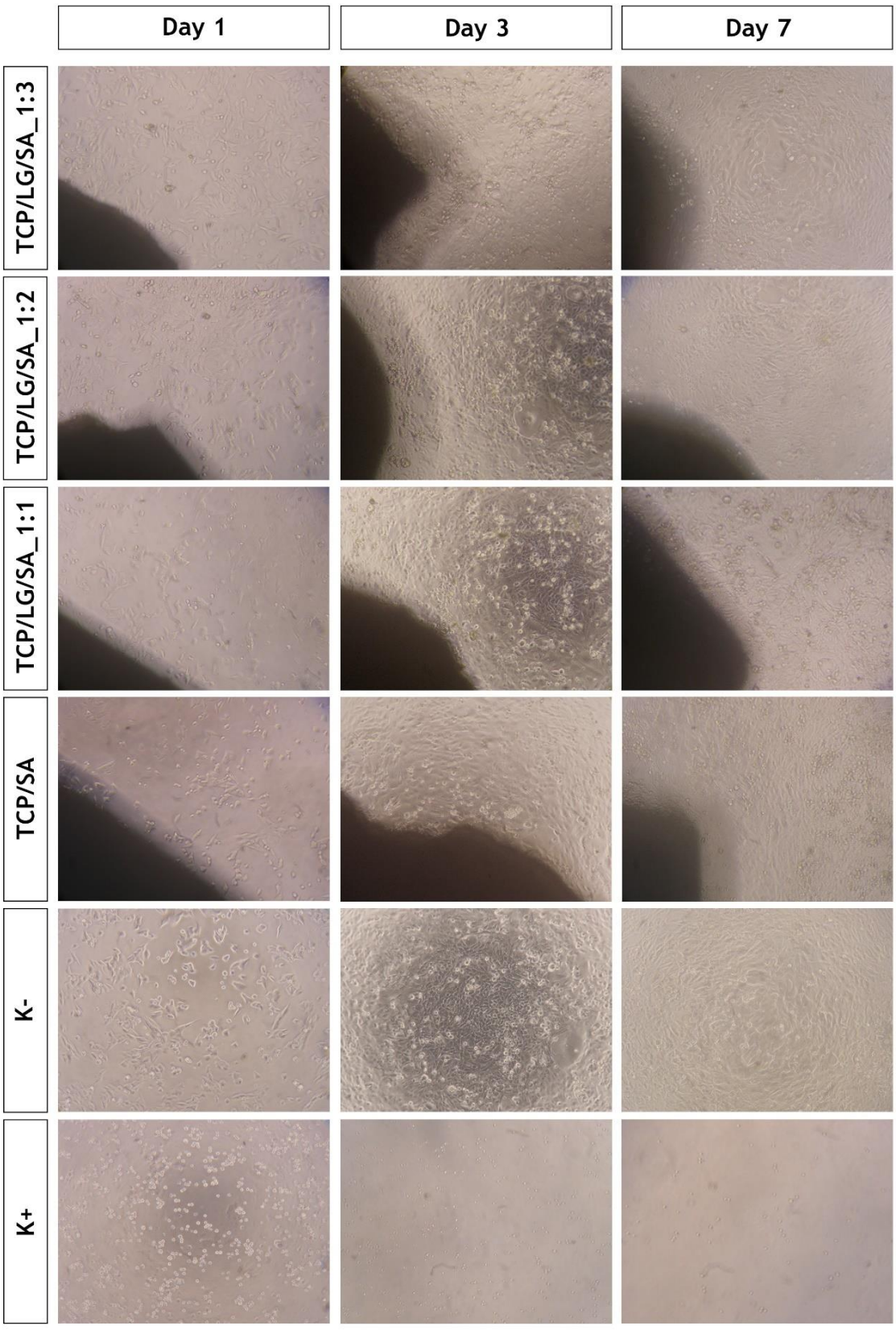

Figure 16. Optical microscopy images acquired to characterize cells' behaviour in contact with the produced scaffolds during 1, 3 and 7 days. The negative control (K^-) are cells cultured without the scaffolds, and positive control (K^+) are cells incubated with ethanol.

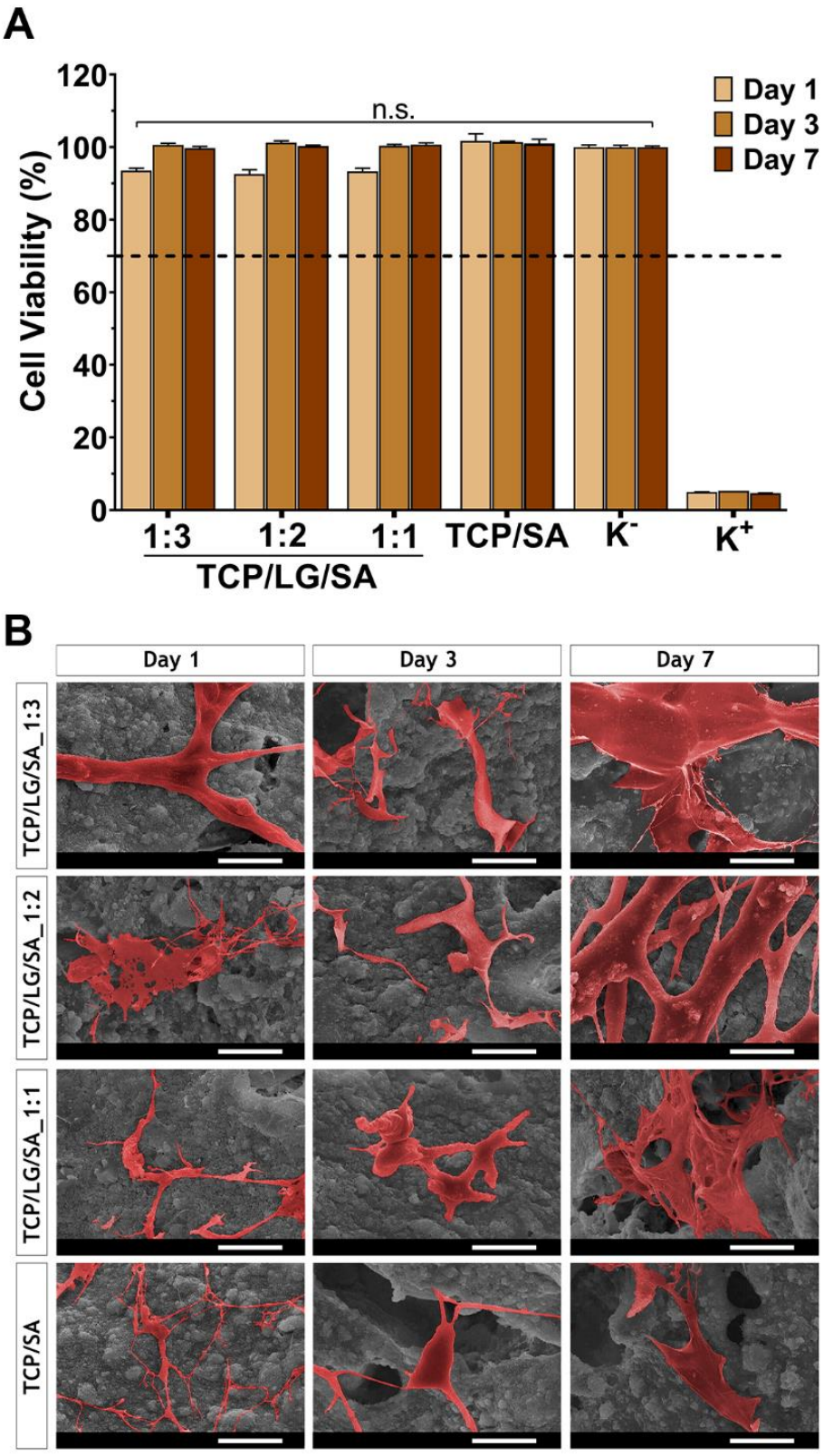

Figure 17. Characterization of the scaffolds' cytocompatibility. Analysis of the cellular viability profile of hOB incubated in the presence of the 3D scaffolds through the resazurin assay at 1, 3, and 7 days. Positive control (K^+) are cells incubated with ethanol, and the negative control (K^-) are cells cultured without the scaffolds. Data are presented as the mean ±standard deviation, n = 5; n.s. - not statistically significant (A). Representative pseudo-colored SEM images of hOB cells seeded on the surface of 3D scaffolds for 1, 3, and 7 days. Scale bars represent 21.3 μm (B).

3.8.2 Evaluation *in vitro* biomineralization

The 3D scaffolds' ability to promote/support the deposition of minerals is an important step for promoting the full regeneration of the bone. Particularly, the fixation of PO_4^{-3} and Ca^{2+} contributes to the formation of calcium phosphate crystals, namely in the form of hydroxyapatite ($Ca_5(PO_4)_3(OH)$) [142]. Thus, the scaffolds' biomineralization upon incubation in SBF was evaluated over a period of 21 days. For this purpose, the formation of apatite crystals on the scaffolds' surface was monitored through SEM (Figure 18 A). The SEM images demonstrate the initial deposition of hydroxyapatite nanocrystals that continued to grow and formed plates at all the 3D scaffolds formulations with the progression of the incubation time.

Furthermore, the ARS staining evaluated the scaffolds' matrix mineralization when in the presence of hOB cells for 1, 3, 7, and 14 days (Figure 18 B). The obtained results further corroborated the cytocompatibility findings that the LG addition does not compromise the scaffolds' biological performance, namely the osteogenic capacity. In fact, at all time points the TCP/LG/SA_1:3, TCP/LG/SA_1:2, TCP/LG/SA_1:1 scaffolds showed a similar ARS concentration to that obtained in TCP/SA scaffolds. In summary, the osteogenic properties can be mainly attributed to the TCP's intrinsic capacity to stimulate biomineralization, and consequently, facilitate the osteointegration of the 3D scaffolds. Moreover, this enhanced biomineralization of TCP/LG/SA and TCP/SA scaffolds is in agreement with other reports in the literature where similar polymer/ceramic matrices were used for bone tissue regeneration [79, 117]. Wang *et al.* produced LG/PCL nanofibers and observed that these structures could mediate the formation of HAp crystals and consequent biomineralization [143]. Moreover, Boga and colleagues also reported that TCP/alginic acid 3D printed scaffolds act as supports for the mineral deposition leading to the formation of HAp crystals during 21 days [123].

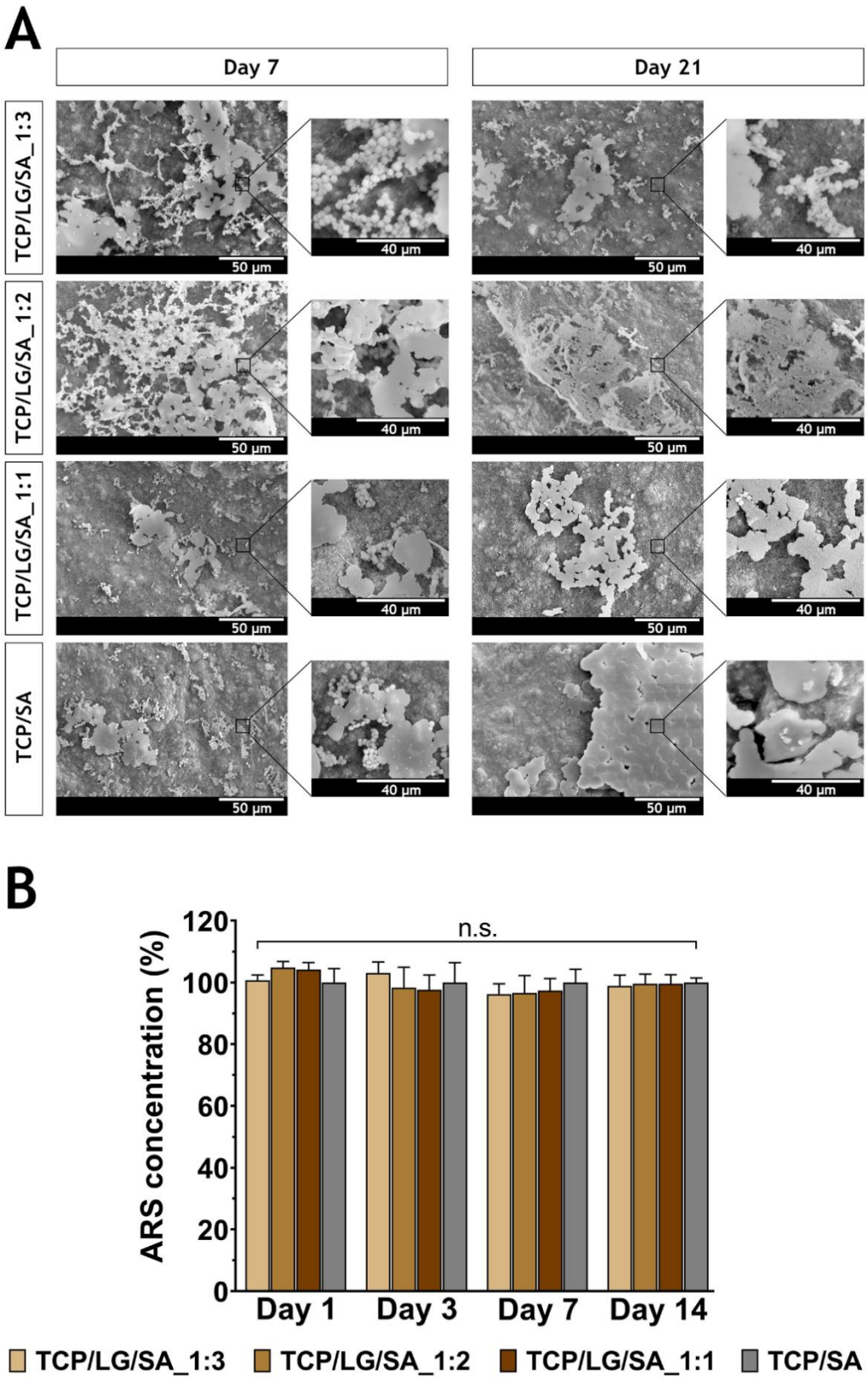

Figure 18. Characterization of the scaffolds' biomineralization. Representative SEM images of the apatite deposition on the surface of TCP/LG/SA_1:3, TCP/LG/SA_1:2, TCP/LG/SA_1:1, and TCP/SA scaffolds (A). Analysis of the ARS concentration after 3D scaffolds incubation in the presence of hOB cells for 1, 3, 7, and 14 days. Data are presented as the mean ±standard deviation, n = 6; n.s. - not statistically significant (B).

Chapter 4

Conclusion and Future Perspectives

4. Conclusion and Future Perspectives

The development of 3D scaffolds for bone regeneration aims to create permanent or temporary replacements that mimic the structural composition of native bone, *i.e.*, composite materials with organic and inorganic phases. Moreover, the 3D scaffolds must also present physicochemical properties capable of stabilizing the bone lesion and enhancing the new bone formation (*e.g.*, cell adhesion, proliferation, and differentiation). Therefore, the constitution and desired bioactivity of the 3D scaffolds was taken into consideration when selecting the biomaterials to use: the TCP provides mechanical and osteogenic properties; SA provides biodegradability and biocompatibility, and LG can further boost the scaffolds' mechanical resistance.

In this master's dissertation, a new 3D scaffold was produced, based on the TCP/LG/SA combination and layer-by-layer extrusion using a Fab@Home 3D-plotter. Three different TCP/LG/SA scaffolds were produced by varying the LG/SA ratio (*i.e.*, 1:3, 1:2, and 1:1) and compared with the TCP/SA scaffolds. The results demonstrated that the LG inclusion improved the mechanical resistance of the scaffolds, particularly the TCP/LG/SA_1:2 scaffolds showed an ≈ 15 % increase in the *Cs*. Moreover, it was also observed an increase in the WCA of the TCP/LG/SA scaffolds, presenting values closer to that considered ideal for biological applications. Furthermore, the TCP/LG/SA scaffolds presented high biocompatibility during the 7 days of study. Additionally, the SEM images confirmed the capacity of the hOB cells to adhere and proliferate at the scaffolds surface, further corroborating that the LG inclusion does not present any toxic effect on the cells. Otherwise, no significant differences were observed in the calcium deposition at the surface of TCP/LG/SA and TCP/SA scaffolds. Altogether, the results support the inclusion of LG in the 3D scaffolds for bone regeneration, originating stronger structures with more suitable environments for cell adhesion and proliferation. Moreover, it is worth noticing, that to the best of our knowledge this is one of the first works exploring the LG application to reinforce TCP/SA scaffolds.

In the future, osteopontin, osteocalcin, and BMP-2 expression assays should be performed to further characterize the osteoinductive and osteoconductive properties of TCP/LG/SA scaffolds. Moreover, the introduction of stem cells and/or bioactive molecules (*e.g.*, growth factors and bone morphogenic proteins) to TCP/LG/SA mixture before the printing process may be pursued to enhance the 3D scaffolds' functionality and the bone healing process. Following that, the *in vivo* performance of TCP/LG/SA scaffolds will be essential to validate their potential for bone healing applications.

Chapter 5

References

5. References

[1] G. Zhu, T. Zhang, M. Chen, K. Yao, X. Huang, B. Zhang, Y. Li, J. Liu, Y. Wang, Z. Zhao, Bone physiological microenvironment and healing mechanism: Basis for future bone-tissue engineering scaffolds, Bioact. Mater., 6 (2021) 4110-4140.

[2] M. Filippi, G. Born, M. Chaaban, A. Scherberich, Natural polymeric scaffolds in bone regeneration, Front. Bioeng. Biotechnol., 8 (2020) 474.

[3] X. Wang, S. Xu, S. Zhou, W. Xu, M. Leary, P. Choong, M. Qian, M. Brandt, Y.M. Xie, Topological design and additive manufacturing of porous metals for bone scaffolds and orthopaedic implants: A review, Biomaterials, 83 (2016) 127-141.

[4] N. Su, J. Yang, Y. Xie, X. Du, H. Chen, H. Zhou, L. Chen, Bone function, dysfunction and its role in diseases including critical illness, Int. J. Biol. Sci., 15 (2019) 776.

[5] E.F. Morgan, G.L. Barnes, T.A. Einhorn, Chapter 1 - The Bone Organ System: Form and Function, in: R. Marcus, D. Feldman, Osteoporosis (Fourth Edition), Academic Press, (2013) 3-20.

[6] B.D. Boyan, C.H. Lohmann, J. Romero, Z. Schwartz, Bone and cartilage tissue engineering, Clin Plast Surg., 26 (1999) 629-645.

[7] B.M. Manzini, L.M.R. Machado, P.Y. Noritomi, J.V.L. da Silva, Advances in Bone tissue engineering: A fundamental review, J. BioSci., 46 (2021) 1-18.

[8] H.F. Pereira, I.F. Cengiz, F.S. Silva, R.L. Reis, J.M. Oliveira, Scaffolds and coatings for bone regeneration, J. Mater. Sci.: Mater. Med., 31 (2020) 1-16.

[9] R.R. Seeley, T.D.Stephens, P.Tate, Anatomy & Physiology, McGraw-Hill (2003).

[10] M.J.F. Blumer, Bone tissue and histological and molecular events during development of the long bones, Annals of Anatomy - Anatomischer Anzeiger, 235 (2021) 151704.

[11] N.H. Hart, R.U. Newton, J. Tan, T. Rantalainen, P. Chivers, A. Siafarikas, S. Nimphius, Biological basis of bone strength: anatomy, physiology and measurement, J. Musculoskeletal Neuronal Interact., 20 (2020) 347-371.

[12] E. Bilgiç, Ö. Boyacıoğlu, M. Gizer, P. Korkusuz, F. Korkusuz, Chapter 6 - Architecture of bone tissue and its adaptation to pathological conditions, Comparative Kinesiology of the Human Body, Academic Press, (2020) 71-90.

[13] R. Oftadeh, M. Perez-Viloria, J.C. Villa-Camacho, A. Vaziri, A. Nazarian, Biomechanics and mechanobiology of trabecular bone: a review, J. Biomech. Eng., 137 (2015).

[14] T.L. Kivell, A review of trabecular bone functional adaptation: what have we learned from trabecular analyses in extant hominoids and what can we apply to fossils?, J. Anat., 228 (2016) 569-594.

[15] L.M. McNamara, 2.10 Bone as a Material, Comprehensive Biomaterials II, Elsevier, (2017) 202-227.

[16] R. Florencio-Silva, G.R.d.S. Sasso, E. Sasso-Cerri, M.J. Simões, P.S. Cerri, Biology of bone tissue: structure, function, and factors that influence bone cells, BioMed Res. Int., 2015 (2015).

[17] P. Chocholata, V. Kulda, V. Babuska, Fabrication of scaffolds for bone-tissue regeneration, Materials, 12 (2019) 568.

[18] X. Lin, S. Patil, Y.-G. Gao, A. Qian, The bone extracellular matrix in bone formation and regeneration, Front. Pharmacol., 11 (2020) 757.

[19] R. Florencio-Silva, G.R.d.S. Sasso, E. Sasso-Cerri, M.J. Simões, P.S. Cerri, Biology of Bone Tissue: Structure, Function, and Factors That Influence Bone Cells, BioMed Research International, 2015 (2015) 421746.

[20] R.K. Fuchs, W.R. Thompson, S.J. Warden, 2 - Bone biology, Bone Repair Biomaterials (Second Edition), Woodhead Publishing Series in Biomaterials, (2019) 15-52.

[21] M. Ansari, Bone tissue regeneration: biology, strategies and interface studies, Prog. Biomater., 8 (2019) 223-237.

[22] A. Salhotra, H.N. Shah, B. Levi, M.T. Longaker, Mechanisms of bone development and repair, Nat. Rev. Mol. Cell Biol., 21 (2020) 696-711.

[23] J.O. Hollinger, P. Alvarez-Urena, P. Ducheyne, A. Srinivasan, J. Baskin, H. Waters, R. Gruber, 6.2 Bone Tissue Engineering: Growth Factors and Cytokines, Comprehensive Biomaterials II, Elsevier, (2017) 20-53.

[24] N. Dirckx, M.C. Moorer, T.L. Clemens, R.C. Riddle, The role of osteoblasts in energy homeostasis, Nat. Rev. Endocrinol., 15 (2019) 651-665.

[25] J.P. Henry, B. Bordoni, Histology, Osteoblasts, StatPearls [Internet], StatPearls Publishing, (2022).

[26] M. Hayashi, T. Ono, T. Nakashima, Signaling in Osteoblast Differentiation, Encyclopedia of Bone Biology, Academic Press, (2020), 416-426.

[27] S. Bolamperti, I. Villa, A. Rubinacci, Bone remodeling: an operational process ensuring survival and bone mechanical competence, Bone Res., 10 (2022) 1-19.

[28] J.L. Brown, S.G. Kumbar, C.T. Laurencin, Chapter II.6.7 - Bone Tissue Engineering, Biomaterials Science (Third Edition), Academic Press, (2013) 1194-1214.

[29] E. Dall'Ara, V.S. Cheong, Chapter 6 - Bone biomechanics, Human Orthopaedic Biomechanics, Academic Press, (2022), 97-120.

[30] F.G.F. Tresguerres, J. Torres, J. López-Quiles, G. Hernández, J.A. Vega, I.F. Tresguerres, The osteocyte: A multifunctional cell within the bone, Annals of Anatomy - Anatomischer Anzeiger, 227 (2020) 151422.

[31] M.B. Schaffler, W.-Y. Cheung, R. Majeska, O. Kennedy, Osteocytes: master orchestrators of bone, Calcif. Tissue Int., 94 (2014) 5-24.

[32] H. Chen, T. Senda, K.-y. Kubo, The osteocyte plays multiple roles in bone remodeling and mineral homeostasis, Med. Mol. Morphol., 48 (2015) 61-68.

[33] T. Ono, T. Nakashima, Recent advances in osteoclast biology, Histochemistry and cell biology, 149 (2018) 325-341.

[34] J. Feher, 9.8 - Calcium and Phosphorus Homeostasis II: Target Tissues and Integrated Control, Quantitative Human Physiology (Second Edition), Academic Press, (2017) 933-945.

[35] A. Ho-Shui-Ling, J. Bolander, L.E. Rustom, A.W. Johnson, F.P. Luyten, C. Picart, Bone regeneration strategies: Engineered scaffolds, bioactive molecules and stem cells current stage and future perspectives, Biomaterials, 180 (2018) 143-162.

[36] F. Loi, L.A. Córdova, J. Pajarinen, T.-h. Lin, Z. Yao, S.B. Goodman, Inflammation, fracture and bone repair, Bone, 86 (2016) 119-130.

[37] R. Agarwal, A.J. García, Biomaterial strategies for engineering implants for enhanced osseointegration and bone repair, Adv. Drug Delivery Rev., 94 (2015) 53-62.

[38] R. Marsell, T.A. Einhorn, The biology of fracture healing, Injury, 42 (2011) 551-555.

[39] G. Marongiu, A. Dolci, M. Verona, A. Capone, The biology and treatment of acute long-bones diaphyseal fractures: Overview of the current options for bone healing enhancement, Bone Rep., 12 (2020) 100249.

[40] R. Kaderly, Primary bone healing, Vet. Med. Surg. Small. Anim., (1991). 21-25.

[41] C.S. Bahney, R.L. Zondervan, P. Allison, A. Theologis, J.W. Ashley, J. Ahn, T. Miclau, R.S. Marcucio, K.D. Hankenson, Cellular biology of fracture healing, J. Orthop. Res., 37 (2019) 35-50.

[42] W. Wang, K.W. Yeung, Bone grafts and biomaterials substitutes for bone defect repair: A review, Bioact. Mater., 2 (2017) 224-247.

[43] J.R. Sheen, V.V. Garla, Fracture healing overview, StatPearls [Internet], StatPearls Publishing, (2021).

[44] W. Wang, K.W.K. Yeung, Bone grafts and biomaterials substitutes for bone defect repair: A review, Bioact. Mater., 2 (2017) 224-247.

[45] M. Pfeiffenberger, A. Damerau, A. Lang, F. Buttgereit, P. Hoff, T. Gaber, Fracture Healing Research—Shift towards In Vitro Modeling?, Biomedicines, 9 (2021) 748.

[46] V. Campana, G. Milano, E. Pagano, M. Barba, C. Cicione, G. Salonna, W. Lattanzi, G. Logroscino, Bone substitutes in orthopaedic surgery: from basic science to clinical practice, J. Mater. Sci.: Mater. Med., 25 (2014) 2445-2461.

[47] H.J. Haugen, S.P. Lyngstadaas, F. Rossi, G. Perale, Bone grafts: which is the ideal biomaterial?, J. Clin. Periodontol., 46 (2019) 92-102.

[48] S. Caddeo, M. Boffito, S. Sartori, Tissue engineering approaches in the design of healthy and pathological in vitro tissue models, Front. Bioeng. Biotechnol., 5 (2017) 40.

[49] R. Langer, J. Vacanti, Advances in tissue engineering, J. Pediatr. Surg., 51 (2016) 8-12.

[50] V. Kesireddy, F.K. Kasper, Approaches for building bioactive elements into synthetic scaffolds for bone tissue engineering, J. Mater. Chem. B, 4 (2016) 6773-6786.

[51] M. Alonzo, F. Alvarez Primo, S. Anil Kumar, J.A. Mudloff, E. Dominguez, G. Fregoso, N. Ortiz, W.M. Weiss, B. Joddar, Bone tissue engineering techniques, advances, and scaffolds for treatment of bone defects, Curr. Opin. Biomed. Eng., 17 (2021) 100248.

[52] A.R. Amini, C.T. Laurencin, S.P. Nukavarapu, Bone tissue engineering: recent advances and challenges, Crit. Rev. Biomed. Eng., 40 (2012).

[53] T. Ghassemi, A. Shahroodi, M.H. Ebrahimzadeh, A. Mousavian, J. Movaffagh, A. Moradi, Current concepts in scaffolding for bone tissue engineering, Arch. Bone Jt. Surg., 6 (2018) 90.

[54] M.P. Nikolova, M.S. Chavali, Recent advances in biomaterials for 3D scaffolds: A review, Bioact. Mater., 4 (2019) 271-292.

[55] N. Sultana, 1 - Mechanical and biological properties of scaffold materials, Functional 3D Tissue Engineering Scaffolds, Materials, Technologies and Applications, (2018)1-21.

[56] T. Nardo, I. Carmagnola, F. Ruini, S. Caddeo, S. Calzone, V. Chiono, G. Ciardelli, Chapter 65 - Synthetic Biomaterial for Regenerative Medicine Applications, in: G. Orlando, G. Remuzzi, D.F. Williams (Eds.) Kidney Transplantation, Bioengineering and Regeneration, Academic Press, (2017)901-921.

[57] P. Goswami, T. O'Haire, 3 - Developments in the use of green (biodegradable), recycled and biopolymer materials in technical nonwovens, Advances in Technical Nonwovens, Woodhead Publishing, (2016) 97-114.

[58] C.I. Codrea, A.-M. Croitoru, C.C. Baciu, A. Melinescu, D. Ficai, V. Fruth, A. Ficai, Advances in osteoporotic bone tissue engineering, J. Clin. Med., 10 (2021) 253.

[59] I. Bružauskaitė, D. Bironaitė, E. Bagdonas, E. Bernotienė, Scaffolds and cells for tissue regeneration: different scaffold pore sizes—different cell effects, Cytotechnology, 68 (2016) 355-369.

[60] S. Bose, M. Roy, A. Bandyopadhyay, Recent advances in bone tissue engineering scaffolds, Trends Biotechnol., 30 (2012) 546-554.

[61] L. Polo-Corrales, M. Latorre-Esteves, J.E. Ramirez-Vick, Scaffold design for bone regeneration, J. Nanosci. Nanotechnol., 14 (2014) 15-56.

[62] F.J. O'Brien, Biomaterials & scaffolds for tissue engineering, Mater. Today, 14 (2011) 88-95.

[63] E.F. Morgan, G.U. Unnikrisnan, A.I. Hussein, Bone mechanical properties in healthy and diseased states, Annu. Rev. Biomed. Eng., 20 (2018) 119-143.

[64] X. Zhang, X.-W. Li, J.-G. Li, X.-D. Sun, Preparation and mechanical property of a novel 3D porous magnesium scaffold for bone tissue engineering, Mater. Sci. Eng. C, 42 (2014) 362-367.

[65] L.-C. Gerhardt, A.R. Boccaccini, Bioactive Glass and Glass-Ceramic Scaffolds for Bone Tissue Engineering, Materials, 3 (2010) 3867-3910.

[66] S. Mohamed, B.H. Shamaz, Bone tissue engineering and bony scaffolds, Int. J. Dent. Oral Health, 1 (2015) 15-20.

[67] V. Karageorgiou, D. Kaplan, Porosity of 3D biomaterial scaffolds and osteogenesis, Biomaterials, 26 (2005) 5474-5491.

[68] D. Zhao, Y. Huang, Y. Ao, C. Han, Q. Wang, Y. Li, J. Liu, Q. Wei, Z. Zhang, Effect of pore geometry on the fatigue properties and cell affinity of porous titanium scaffolds fabricated by selective laser melting, J. Mech. Behav. Biomed. Mater., 88 (2018) 478-487.

[69] C.T. Johnson, A.J. García, Scaffold-based anti-infection strategies in bone repair, Ann. Biomed. Eng., 43 (2015) 515-528.

[70] A.R. Unnithan, R.S. Arathyram, C.S. Kim, Chapter 7 - Scaffolds with Antibacterial Properties, Nanotechnology Applications for Tissue Engineering, William Andrew Publishing, (2015) 103-123.

[71] M. Álvarez-Paino, A. Muñoz-Bonilla, M. Fernández-García, Antimicrobial polymers in the nano-world, Nanomater., 7 (2017) 48.

[72] G. Turnbull, J. Clarke, F. Picard, P. Riches, L. Jia, F. Han, B. Li, W. Shu, 3D bioactive composite scaffolds for bone tissue engineering, Bioact. Mater., 3 (2018) 278-314.

[73] M.S.B. Reddy, D. Ponnamma, R. Choudhary, K.K. Sadasivuni, A comparative review of natural and synthetic biopolymer composite scaffolds, Polym., 13 (2021) 1105.

[74] A.V. Do, B. Khorsand, S.M. Geary, A.K. Salem, 3D printing of scaffolds for tissue regeneration applications, Adv. Healthcare Mater., 4 (2015) 1742-1762.

[75] B. Yuan, S.-y. Zhou, X.-s. Chen, Rapid prototyping technology and its application in bone tissue engineering, J. Zhejiang Univ. Sci. B, 18 (2017) 303-315.

[76] S. Sohn, M.V. Buskirk, M.J. Buckenmeyer, R. Londono, D. Faulk, Whole organ engineering: approaches, challenges, and future directions, Appl. Sci., 10 (2020) 4277.

[77] X. Wang, Z. Wang, W. Zhai, F. Wang, Z. Ge, H. Yu, W. Yang, Engineering biological tissues from the bottom-up: Recent advances and future prospects, Micromachines, 13 (2021) 75.

[78] A. Pandey, G. Singh, S. Singh, K. Jha, C. Prakash, 3D printed biodegradable functional temperature-stimuli shape memory polymer for customized scaffoldings, J. Mech. Behav. Biomed. Mater., 108 (2020) 103781.

[79] R. Fradique, T.R. Correia, S. Miguel, K. De Sa, D. Figueira, A. Mendonça, I. Correia, Production of new 3D scaffolds for bone tissue regeneration by rapid prototyping, J. Mater. Sci.: Mater. Med., 27 (2016) 1-14.

[80] K. Kang, L. Hockaday, J. Butcher, Quantitative optimization of solid freeform deposition of aqueous hydrogels, Biofabrication, 5 (2013) 035001.

[81] M.N. Collins, G. Ren, K. Young, S. Pina, R.L. Reis, J.M. Oliveira, Scaffold fabrication technologies and structure/function properties in bone tissue engineering, Adv. Funct. Mater., 31 (2021) 2010609.

[82] J.G. Lyons, M.A. Plantz, W.K. Hsu, E.L. Hsu, S. Minardi, Nanostructured biomaterials for bone regeneration, Front. Bioeng. Biotechnol., 8 (2020) 922.

[83] M.R. Cohn, A. Unnanuntana, T.J. Pannu, S.J. Warner, J.M. Lane, 7.16 Materials in Fracture Fixation, Comprehensive Biomaterials II, Elsevier, (2017) 278-297.

[84] B. Huang, G. Caetano, C. Vyas, J.J. Blaker, C. Diver, P. Bártolo, Polymer-ceramic composite scaffolds: The effect of hydroxyapatite and β-tri-calcium phosphate, Materials, 11 (2018) 129.

[85] C.F. Santos, A.P. Silva, L. Lopes, I. Pires, I.J. Correia, Design and production of sintered β-tricalcium phosphate 3D scaffolds for bone tissue regeneration, Mater. Sci. Eng. C, 32 (2012) 1293-1298.

[86] H. Lu, Y. Zhou, Y. Ma, L. Xiao, W. Ji, Y. Zhang, X. Wang, Current application of beta-tricalcium phosphate in bone repair and its mechanism to regulate osteogenesis, Front. Mater., (2021) 277.

[87] J.E. Jeong, S.Y. Park, J.Y. Shin, J.M. Seok, J.H. Byun, S.H. Oh, W.D. Kim, J.H. Lee, W.H. Park, S.A. Park, 3D Printing of Bone-Mimetic Scaffold Composed of Gelatin/β-Tri-Calcium Phosphate for Bone Tissue Engineering, Macromol. Biosci., 20 (2020) 2000256.

[88] H.J. Park, K.D. Min, M.C. Lee, S.H. Kim, O.J. Lee, H.W. Ju, B.M. Moon, J.M. Lee, Y.R. Park, D.W. Kim, Fabrication of 3D porous SF/β-TCP hybrid scaffolds for bone tissue reconstruction, J. Biomed. Mater. Res., Part A, 104 (2016) 1779-1787.

[89] V. Saxena, I. Shukla, L.M. Pandey, Chapter 8 - Hydroxyapatite: an inorganic ceramic for biomedical applications, Materials for Biomedical Engineering, Elsevier, (2019) 205-249.

[90] E. Fiume, G. Magnaterra, A. Rahdar, E. Verné, F. Baino, Hydroxyapatite for biomedical applications: a short overview, Ceram., 4 (2021) 542-563.

[91] H. Nosrati, R. Sarraf Mamoory, D.Q. Svend Le, C.E. Bünger, Fabrication of gelatin/hydroxyapatite/3D-graphene scaffolds by a hydrogel 3D-printing method, Mater. Chem. Phys., 239 (2020) 122305.

[92] S.C. Cox, J.A. Thornby, G.J. Gibbons, M.A. Williams, K.K. Mallick, 3D printing of porous hydroxyapatite scaffolds intended for use in bone tissue engineering applications, Mater. Sci. Eng. C, 47 (2015) 237-247.

[93] B. ter Horst, N.S. Moiemen, L.M. Grover, 6 - Natural polymers: biomaterials for skin scaffolds, Biomaterials for Skin Repair and Regeneration, Woodhead Publishing, (2019) 151-192.

[94] Z. Gao, X. Lang, S. Chen, C. Zhao, Mini-Review on the Synthesis of Lignin-Based Phenolic Resin, Energy Fuels, 35 (2021) 18385-18395.

[95] L.A. Loureiro dos Santos, Natural Polymeric Biomaterials: Processing and Properties, Reference Module in Materials Science and Materials Engineering, Elsevier, 2017.

[96] F. Liu, Q. Chen, C. Liu, Q. Ao, X. Tian, J. Fan, H. Tong, X. Wang, Natural polymers for organ 3D bioprinting, Polym., 10 (2018) 1278.

[97] A. Ahmad, N. Mubarak, F.T. Jannat, T. Ashfaq, C. Santulli, M. Rizwan, A. Najda, M. Bin-Jumah, M.M. Abdel-Daim, S. Hussain, A critical review on the synthesis of natural sodium alginate based composite materials: An innovative biological polymer for biomedical delivery applications, Processes, 9 (2021) 137.

[98] Y. Wang, X. Wang, J. Shi, R. Zhu, J. Zhang, Z. Zhang, D. Ma, Y. Hou, F. Lin, J. Yang, A biomimetic silk fibroin/sodium alginate composite scaffold for soft tissue engineering, Sci. Rep., 6 (2016) 1-13.

[99] R.L.M.S. Oliveira, A.P.N. Alves, L. Barbosa, A.P. Silva, G.L. de Cena, K. Conceição, D.B. Tada, E.d.S. Trichês, 3D printing of bioactive glass S53P4/sodium alginate sintering-free scaffolds, Bioprint., 27 (2022) e00226.

[100] L. Donaldson, B. Nanayakkara, J. Harrington, Wood Growth and Development, Encyclopedia of Applied Plant Sciences (Second Edition), Academic Press, (2017) 203-210.

[101] A. Grossman, W. Vermerris, Lignin-based polymers and nanomaterials, Curr. Opin. Biotechnol., 56 (2019) 112-120.

[102] R. Kumar, A. Butreddy, N. Kommineni, P.G. Reddy, N. Bunekar, C. Sarkar, S. Dutt, V.K. Mishra, K.R. Aadil, Y.K. Mishra, Lignin: drug/gene delivery and tissue engineering applications, Int. J. Nanomed., 16 (2021) 2419.

[103] B. Kim, Y. Kim, Y. Lee, J. Oh, Y. Jung, W.G. Koh, J.J. Chung, Reactive Oxygen Species Suppressive Kraft Lignin-Gelatin based Antioxidant hydrogels for Chronic Wound Repair, Macromol. Biosci., (2022) 2200234.

[104] P. Rejmontová, A. Kovalcik, P. Humpolíček, Z. Capáková, E. Wrzecionko, P. Sáha, The use of fractionated Kraft lignin to improve the mechanical and biological properties of PVA-based scaffolds, RSC Adv., 9 (2019) 12346-12353.

[105] E. Troy, M.A. Tilbury, A.M. Power, J.G. Wall, Nature-Based Biomaterials and Their Application in Biomedicine, Polym., 13 (2021) 3321.

[106] A.M. Ferreira, P. Gentile, V. Chiono, G. Ciardelli, Collagen for bone tissue regeneration, Acta Biomater., 8 (2012) 3191-3200.

[107] Y. Song, H. Wu, Y. Gao, J. Li, K. Lin, B. Liu, X. Lei, P. Cheng, S. Zhang, Y. Wang, Zinc silicate/nano-hydroxyapatite/collagen scaffolds promote angiogenesis and bone regeneration via the p38 MAPK pathway in activated monocytes, ACS Appl. Mater. Interfaces, 12 (2020) 16058-16075.

[108] A. Muxika, A. Etxabide, J. Uranga, P. Guerrero, K. de la Caba, Chitosan as a bioactive polymer: Processing, properties and applications, Int. J. Biol. Macromol., 105 (2017) 1358-1368.

[109] M. Rodríguez-Vázquez, B. Vega-Ruiz, R. Ramos-Zúñiga, D.A. Saldaña-Koppel, L.F. Quiñones-Olvera, Chitosan and its potential use as a scaffold for tissue engineering in regenerative medicine, BioMed Res. Int., 2015 (2015).

[110] I.R. Serra, R. Fradique, M.C.S. Vallejo, T.R. Correia, S.P. Miguel, I.J. Correia, Production and characterization of chitosan/gelatin/β-TCP scaffolds for improved bone tissue regeneration, Mater. Sci. Eng. C, 55 (2015) 592-604.

[111] A. Georgopoulou, F. Papadogiannis, A. Batsali, J. Marakis, K. Alpantaki, A.G. Eliopoulos, C. Pontikoglou, M. Chatzinikolaidou, Chitosan/gelatin scaffolds support bone regeneration, J. Mater. Sci.: Mater. Med., 29 (2018) 1-13.

[112] S. Unal, F.N. Oktar, M. Mahirogullari, O. Gunduz, 9 - Bone structure and formation: A new perspective, Bioceramics, Elsevier, (2021) 175-193.

[113] J.R. Dias, A. Sousa, A. Augusto, P.J. Bártolo, P.L. Granja, Electrospun Polycaprolactone (PCL) Degradation: An In Vitro and In Vivo Study, Polym., 14 (2022) 3397.

[114] D. Mondal, M. Griffith, S.S. Venkatraman, Polycaprolactone-based biomaterials for tissue engineering and drug delivery: Current scenario and challenges, Int. J. Polym. Mater. Polym. Biomater., 65 (2016) 255-265.

[115] A. Zimmerling, Z. Yazdanpanah, D.M. Cooper, J.D. Johnston, X. Chen, 3D printing PCL/nHA bone scaffolds: Exploring the influence of material synthesis techniques, Biomater. Res., 25 (2021) 1-12.

[116] N. Fazeli, E. Arefian, S. Irani, A. Ardeshirylajimi, E. Seyedjafari, 3D-Printed PCL Scaffolds Coated with Nanobioceramics Enhance Osteogenic Differentiation of Stem Cells, ACS Omega, 6 (2021) 35284-35296.

[117] T.R. Correia, D.R. Figueira, K.D. de Sá, S.P. Miguel, R.G. Fradique, A.G. Mendonça, I.J. Correia, 3D printed scaffolds with bactericidal activity aimed for bone tissue regeneration, Int. J. Biol. Macromol., 93 (2016) 1432-1445.

[118] T. Kokubo, H. Takadama, How useful is SBF in predicting in vivo bone bioactivity?, Biomaterials, 27 (2006) 2907-2915.

[119] A. Torres, V. Gaspar, I. Serra, G. Diogo, R. Fradique, A. Silva, I. Correia, Bioactive polymeric–ceramic hybrid 3D scaffold for application in bone tissue regeneration, Mater. Sci. Eng. C, 33 (2013) 4460-4469.

[120] J. Valente, T.A.M. Valente, P. Alves, P. Ferreira, A. Silva, I. Correia, Alginate based scaffolds for bone tissue engineering, Mater. Sci. Eng. C, 32 (2012) 2596-2603.

[121] A.L. Torres, V.M. Gaspar, I.R. Serra, G.S. Diogo, R. Fradique, A.P. Silva, I.J. Correia, Bioactive polymeric–ceramic hybrid 3D scaffold for application in bone tissue regeneration, Mater. Sci. Eng. C, 33 (2013) 4460-4469.

[122] H. Jiankang, L. Dichen, L. Yaxiong, Y. Bo, L. Bingheng, L. Qin, Fabrication and characterization of chitosan/gelatin porous scaffolds with predefined internal microstructures, Polymer, 48 (2007) 4578-4588.

[123] J.C. Boga, S.P. Miguel, D. de Melo-Diogo, A.G. Mendonça, R.O. Louro, I.J. Correia, In vitro characterization of 3D printed scaffolds aimed at bone tissue regeneration, Colloids Surf., B, 165 (2018) 207-218.

[124] C.S.D. Cabral, S.P. Miguel, D. de Melo-Diogo, R.O. Louro, I.J. Correia, Green reduced graphene oxide functionalized 3D printed scaffolds for bone tissue regeneration, Carbon, 146 (2019) 513-523.

[125] Y. Du, J.L. Guo, J. Wang, A.G. Mikos, S. Zhang, Hierarchically designed bone scaffolds: From internal cues to external stimuli, Biomaterials, 218 (2019) 119334.

[126] K. Rechendorff, M.B. Hovgaard, M. Foss, V. Zhdanov, F. Besenbacher, Enhancement of protein adsorption induced by surface roughness, Langmuir, 22 (2006) 10885-10888.

[127] A.R. Calore, V. Srinivas, L. Groenendijk, A. Serafim, I.C. Stancu, A. Wilbers, N. Leoné, A.A. Sanchez, D. Auhl, C. Mota, K. Bernaerts, J.A.W. Harings, L. Moroni, Manufacturing of scaffolds with interconnected internal open porosity and surface roughness, Acta Biomater., (2022).

[128] P. Sotiropoulou, G. Fountos, N. Martini, V. Koukou, C. Michail, I. Kandarakis, G. Nikiforidis, Bone calcium/phosphorus ratio determination using dual energy X-ray method, Phys. Med., 31 (2015) 307-313.

[129] L. Bi, W. Cheng, H. Fan, G. Pei, Reconstruction of goat tibial defects using an injectable tricalcium phosphate/chitosan in combination with autologous platelet-rich plasma, Biomaterials, 31 (2010) 3201-3211.

[130] M. Castilho, J. Rodrigues, I. Pires, B. Gouveia, M. Pereira, C. Moseke, J. Groll, A. Ewald, E. Vorndran, Fabrication of individual alginate-TCP scaffolds for bone tissue engineering by means of powder printing, Biofabrication, 7 (2015) 015004.

[131] L. Tao, L. Zhonglong, X. Ming, Y. Zezheng, L. Zhiyuan, Z. Xiaojun, W. Jinwu, In vitro and in vivo studies of a gelatin/carboxymethyl chitosan/LAPONITE® composite scaffold for bone tissue engineering, RSC Adv., 7 (2017) 54100-54110.

[132] G. Diogo, V. Gaspar, I. Serra, R. Fradique, I. Correia, Manufacture of β-TCP/alginate scaffolds through a Fab@ home model for application in bone tissue engineering, Biofabrication, 6 (2014) 025001.

[133] S. Guo, X. Zhu, M. Li, L. Shi, J.L.T. Ong, D. Jańczewski, K.G. Neoh, Parallel control over surface charge and wettability using polyelectrolyte architecture: effect on protein adsorption and cell adhesion, ACS Appl. Mater. Interfaces, 8 (2016) 30552-30563.

[134] S.M. Oliveira, N.M. Alves, J.F. Mano, Cell interactions with superhydrophilic and superhydrophobic surfaces, J. Adhes. Sci. Technol., 28 (2014) 843-863.

[135] D.P. Dowling, I.S. Miller, M. Ardhaoui, W.M. Gallagher, Effect of surface wettability and topography on the adhesion of osteosarcoma cells on plasma-modified polystyrene, J. Biomater. Appl., 26 (2011) 327-347.

[136] M. Mohammadalipour, T. Behzad, S. Karbasi, Z. Mohammadalipour, Optimization and characterization of polyhydroxybutyrate/lignin electro-spun scaffolds for tissue engineering applications, Int. J. Biol. Macromol., 218 (2022) 317-334.

[137] S.J. Hollister, Porous scaffold design for tissue engineering, Nat. Mater., 4 (2005) 518-524.

[138] J. Diao, J. OuYang, T. Deng, X. Liu, Y. Feng, N. Zhao, C. Mao, Y. Wang, 3D-plotted beta-tricalcium phosphate scaffolds with smaller pore sizes improve in vivo bone regeneration and biomechanical properties in a critical-sized calvarial defect rat model, Adv. Healthcare Mater., 7 (2018) 1800441.

[139] B. Zhu, H. Yin, Alginate lyase: Review of major sources and classification, properties, structure-function analysis and applications, Bioengineered, 6 (2015) 125-131.

[140] P. Picart, P.D. de María, A. Schallmey, From gene to biorefinery: microbial β-etherases as promising biocatalysts for lignin valorization, Front. Microbiol., 6 (2015) 916.

[141] W.-X. Cheng, Y.-Z. Liu, X.-B. Meng, Z.-T. Zheng, L.-L. Li, L.-Q. Ke, L. Li, C.-S. Huang, G.-Y. Zhu, H.-D. Pan, L. Qin, X.-L. Wang, P. Zhang, PLGA/β-TCP composite scaffold incorporating cucurbitacin B promotes bone regeneration by inducing angiogenesis, J. Orthop. Translat., 31 (2021) 41-51.

[142] H.C. Blair, Q.C. Larrouture, Y. Li, H. Lin, D. Beer-Stoltz, L. Liu, R.S. Tuan, L.J. Robinson, P.H. Schlesinger, D.J. Nelson, Osteoblast differentiation and bone matrix formation in vivo and in vitro, Tissue Eng., Part B, 23 (2017) 268-280.

[143] D. Wang, J. Jang, K. Kim, J. Kim, C.B. Park, “Tree to bone”: lignin/polycaprolactone nanofibers for hydroxyapatite biomineralization, Biomacromolecules, 20 (2019) 2684-2693.

Appendix I

Table C1. Data obtained in the EDS analysis of the produced 3D scaffold

	Elements ([a]at.%)					
Sample	C	O	Na	P	Cl	Ca
TCP/LG/SA_1:3	19.18	55.75	0.17	7.07	1.62	16.19
TCP/LG/SA_1:2	22.44	54.51	0.15	5.85	1.78	15.27
TCP/LG/SA_1:1	25.51	54.96	0.13	5.43	1.36	12.60
TCP/SA	19.48	57.62	0.14	5.82	1.70	15.23

[a]at.% - atomic percentage